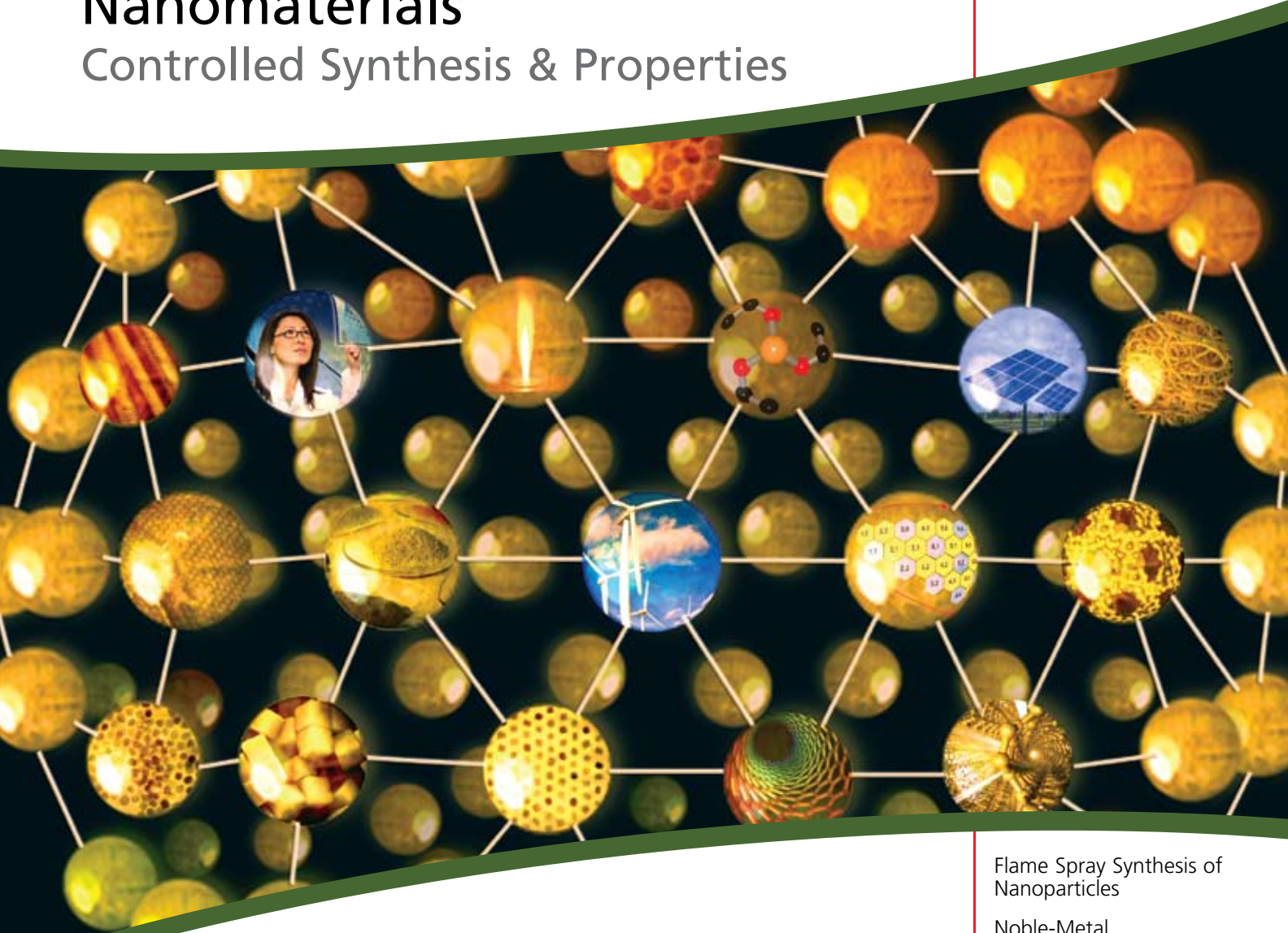


Material Matters™

Vol. 4, No. 1

ALDRICH®
Chemistry

Nanomaterials Controlled Synthesis & Properties



Morphing Materials into Meaning

Flame Spray Synthesis of Nanoparticles

Noble-Metal Nanostructures

Monodisperse Magnetic Nanoparticles

Nanostructured Mesoporous Carbon

Single-Walled Carbon Nanotubes

Introduction

Welcome to the first issue of **Material Matters™** for 2009, which discusses a selection of synthetic methods used to create a variety of nanomaterials, specifically nanoparticles and nanotubes.

A nanomaterial can be broadly defined as any material in which one of its dimensions is less than 100nm. Over the last decade, nanomaterials, including their synthetic methods, have rapidly become one of the most active areas in scientific research, mainly on account of their unique properties in comparison to the traditional micron-sized material. Examples of material properties that change upon entering the nano-regime include conductivity (silicon becomes conductive), transparency (copper becomes transparent), reactivity (aluminium becomes combustible), physical state changes (gold becomes a liquid), and even attainments of chemical behaviors (platinum becomes catalytic).

By studying interactions at the nanoscale, scientists are uncovering fascinating events that aid in the understanding of properties that exist on a quantum level. This knowledge can then be harnessed to develop materials that have an immediate and heightened impact, which affect fields such as alternative energy, electronics and even integrated medicine. The availability of size as a new parameter that permits the tuning of physical and chemical properties has tremendously extended the potential capabilities within materials science.

The in-depth investigation into the properties of these materials is heavily reliant upon the rapid development of synthetic methods that can be used to generate novel nanostructures with reproducible, well-defined features. This issue aims to provide an insight into such controlled synthetic methods and the intriguing materials they can produce.

Researchers in the Department of Chemistry and Applied Biosciences at ETH Zurich describe flame spray synthesis, which is able to produce nanoparticles with a variety of coatings simply by modifying the process parameters. The next article discusses a number of *noble-metal* nanostructures with controlled morphologies that were made using a modified polyol process developed by researchers at Washington University in St. Louis. The synthesis of monodisperse magnetic nanoparticles by researchers at Brown University, is the subject of the next topic, which exemplifies the structures of the nanoparticles made also using a solution-based method. Researchers at the University of York in the UK demonstrate a three-stage heating preparation of mesoporous carbon materials that contain an array of pore diameters. Finally, SouthWest NanoTechnologies, Inc., elaborates on their CoMoCAT® catalytic CVD process, which provide, not only single-walled carbon nanotubes with very narrow diameter distributions but also the ability to scale up production of the highly sought after SWCNTs.

Continuing in the theme of **Material Matters™**, we begin the issue with a section entitled, "Your Materials Matter." Here, we highlight a material that has been brought to our attention by you, the scientific community. Each article in this issue is accompanied by the corresponding Sigma-Aldrich products that are nanomaterials or materials used in the described synthetic processes. The facing page lists the material categories that you will find in this issue. For a comprehensive library of products and all associated information, please visit Aldrich Materials Science at sigma-aldrich.com/matsci. We invite you to direct your comments and questions regarding **Material Matters™** or any materials of interest to matsci@sial.com.

About Our Cover

Nanomaterials are a new class of materials that have been making a silent and, at times, a "not-so" silent revolution in the last decade. A central challenge of nanoscale science is the need for fundamental understanding of how nanomaterials grow and for control of the growth environment, in order to synthesize materials with new or greatly enhanced properties at attractive rates. The cover depicts an artistic rendition of the building block concept in going from synthesis, structure, morphology, to downstream applications—A precursor for magnetic iron oxide nanoparticles, iron(II) ethoxide (as discussed in the article on page 14), a flame to symbolize combustion based processes (presented in the article on page 2), different kinds of nanostructured morphologies and finally to their practical use, be it in solar panels, touch sensitive displays or light-weight, extreme strength nanocomposite-based wind turbines.



Kaushik Patel, Ph.D.
Materials Science Initiative
Sigma-Aldrich Corporation

Material Matters™

Vol. 4 No. 1

Aldrich Chemical Co., Inc.
Sigma-Aldrich Corporation
6000 N. Teutonia Ave.
Milwaukee, WI 53209, USA

To Place Orders

Telephone	800-325-3010 (USA)
FAX	800-325-5052 (USA)

Customer & Technical Services

Customer Inquiries	800-325-3010
Technical Service	800-231-8327
SAFC®	800-244-1173
Custom Synthesis	800-244-1173
Flavors & Fragrances	800-227-4563
International	414-438-3850
24-Hour Emergency	414-438-3850
Web site	sigma-aldrich.com
Email	aldrich@sial.com

Subscriptions

To request your **FREE** subscription to *Material Matters*, please contact us by:

Phone: **800-325-3010 (USA)**

Mail: **Attn: Marketing Communications**
Aldrich Chemical Co., Inc.
Sigma-Aldrich Corporation
P.O. Box 355
Milwaukee, WI 53201-9358

Website: sigma-aldrich.com/mm
Email: sams-usa@sial.com

International customers, please contact your local Sigma-Aldrich office. For worldwide contact information, please see back cover.

Material Matters is also available in PDF format on the Internet at sigma-aldrich.com/matsci.

Aldrich brand products are sold through Sigma-Aldrich, Inc. Sigma-Aldrich, Inc. warrants that its products conform to the information contained in this and other Sigma-Aldrich publications. Purchaser must determine the suitability of the product for its particular use. See reverse side of invoice or packing slip for additional terms and conditions of sale.

All prices are subject to change without notice.

Material Matters (ISSN 1933-9631) is a publication of Aldrich Chemical Co., Inc. Aldrich is a member of the Sigma-Aldrich Group. © 2009 Sigma-Aldrich Co.

"Your Materials Matter."



Joe Porwoll

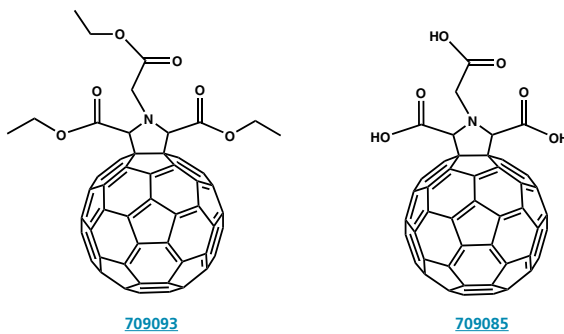
Joe Porwoll, President
Aldrich Chemical Co., Inc.

Do you have a compound that you wish Sigma-Aldrich® could list to help materials research? If it is needed to accelerate your research, it matters—please send your suggestion to matsci@sial.com and we will be happy to give it careful consideration.

Dr. Michael Diener of TDA Research Inc., kindly suggested that we offer the pyrrolidine-derivatized C₆₀ molecule with a tris acid functionality (**Aldrich Prod. No. 709085**). This water-soluble material serves as a superoxide quencher,¹ on account of the redox properties of the C₆₀ moiety. It shows almost 100% improvement in the O₂⁻ quenching activity, which is measured by the decreased levels in reduction of cytochrome c by O₂⁻, (IC₅₀ = 103.4 μM) over analogous water-soluble C₆₀ molecules (IC₅₀ ~ 200 μM).² Fullerene-based compounds therefore have the potential to be patent antioxidants to protect against oxidative stress.³ These materials are expected to play a major part in the fight against Alzheimer's, Parkinson's, AIDS and many other diseases in which oxidation mechanisms play major roles.

References:

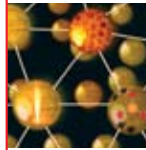
- (1) Okuda, K.; Hirota, T.; Hirobe, M.; Nagano, T.; Mochizuki, M.; Mashino, T. *Fullerene. Sci. Technol.* **2000**, 8, 89-104. (2) Sun, T.; Xu, Z. *Bioorg. Med. Chem. Lett.* **2006**, 16, 3731-3734. (3) Lin, A. M. Y.; Chyi, B. Y.; Wang, S. D.; Yu, H.-H.; Kanakamma, P. P.; Lu, T.-Y.; Chou, C. K.; Ho, L. T. J. *Neurochem.* **1999**, 72, 1634-40.



[709093](#)

[709085](#)

Name	Cat. No.
C ₆₀ Pyrrolidine tris-acid	709085-100MG
C ₆₀ Pyrrolidine tris-acid ethyl ester	709093-250MG



Introduction

Nanomaterials and Nanomaterials Synthesis Products Featured in this Issue

Materials Category	Content	Page
Nanoparticles—Prepared by Nanospray Combustion Process	Nanoparticles prepared via a flame synthesis method	4
Selected Nanoparticles	Selection of additional nanoparticles	5
General Metal Precursors	Precursors used in the synthesis of metal nanoparticles	6
Noble Metal Nanoparticles	A selection of noble metal nanoparticles	11
Noble Metal Precursors	Precursors used in the synthesis of noble metal nanoparticles	11
Capping Agents	Polyvinylpyrrolidones and poly(ethylene glycol)s to control nanoparticle morphology	12
Magnetic Nanoparticles	Nanoparticles with magnetic properties	17
Magnetic Metal Precursors	Precursors used in the synthesis of magnetic nanoparticles	17
Mesoporous Materials	Nanostructured Mesoporous carbons and other mesoporous materials	22
Non-Functionalized Carbon Nanotubes	Single-walled carbon nanotubes (SWNTs), Multi-walled carbon nanotubes (MWNTs) and Nanotube Arrays	27
Functionalized Carbon Nanotubes	SWNTs adorned with a variety of functional groups	28
Fullerenes	A selection of C ₆₀ , C ₇₀ , C ₇₆ and C ₈₄ fullerenes	28



Samuel C. Halim, Robert N. Grass, Wendelin J. Stark*

Institute of Chemical and Bioengineering
Department of Chemistry and Applied Biosciences
ETH Zurich, Switzerland

*Email: wendelin.stark@chem.ethz.ch

How to Make Nanoparticles in Flames

Small-scale materials with particle diameters in the nanometer range have already been used for a long time. The Chinese used carbon black, derived from a combustion process for painting applications a long time before modern technology allowed its industrial production. Besides changing optical properties as described in the above example, nanoparticles can alter physical, optical, electronic or chemical properties of a material by decreasing the particle size. Gold, for instance, is well known for its chemical inertness. Haruta and coworkers showed in the late 80's that even gold becomes a highly active catalyst for CO and H₂ oxidation, if the gold particles are in the nanometer range (**Aldrich Prod. No 636347**).¹ In the past decades there have been thousands of scientific publications covering this area. Due to their changed properties and enhanced reactivity the number of publications discussing nanoparticles has grown exponentially.

There are manifold ways to increase surface area by decreasing the particle size of materials. Generally speaking, there are two approaches toward the synthesis of nanosized materials: *Top-down* approaches such as milling have been known and applied within living memory. Modern milling techniques like ball milling are generally straightforward and can yield nanoparticulate materials. *Bottom-up* techniques include plasma, laser, liquid phase or flame spray synthesis. These "self-assembly" preparation methods generally result in well controlled nanoparticles which are built from smaller building blocks allowing the synthesis of more complex materials or the fabrication of nanoparticles with a very narrow size distribution.

In spite of the often cited novelty of nanomaterials, three large scale commodities have been around for half a century. Large-scale production of these materials started in the early 20th century with the introduction of nanoparticulate carbon black (tire soot) into car tires and rubber. For the large-scale production of silica and pigmentary titania (white pigment) flame technology was further adapted. Both processes are based on the oxidation of chlorides (SiCl₄/TiCl₄) (**Aldrich Prod. Nos. 289388, 254312**) in high temperature flames.² Today, the annual production volumes of flame derived nanoparticles has reached several megatons per year. Major chemical companies have contributed significantly to an efficient process design. Unfortunately, the technology of metal chloride oxidation is only suitable for a very limited set of elements (silicon, aluminum, titanium, vanadium and zirconium). For all other elements—including most mixed element systems—other solutions had to be found. This handicap was overcome initially by Zachariah and Huzarewicz³ as well as Matsoukas and Friedlander⁴ by the use of aqueous precursors. Further optimizations lead to the use of organic precursors like metal alkoxides,⁵ acetates,⁶ triethanolamines,⁷

and metal carboxylates.⁸ The latter is most promising as nearly all elements are available as low-cost naphthenate - metal salts. Further, these metal-organic salts are quite stable in air, tolerate humidity and are freely miscible amongst each other. This allows the fabrication of mixed-oxide materials that have excellent chemical homogeneity⁹ and high batch-to-batch reproducibility (see **Figure 1**).



Figure 1. Using flame spray synthesis, the compositional variety of inorganic nanoparticles is nearly endless. Different oxidic, salt and metallic nanoparticles with similar particle size distribution are depicted (courtesy of Nanograde LLC.).

Laboratory set-ups of flame spray reactors usually operate in the region of 10-100 g/hr (see **Figure 2**) and small pilot plants were shown to be capable of production rates of 1 kg/hr.¹⁰ Today, by the use of liquid organic precursors, the aerosol community has gained access to most oxide materials, and these have been explored for applications in heterogeneous catalysis,^{9,11,12} sensors,¹³ lasing materials,⁷ computer chip manufacturing and numerous other industrial sectors.

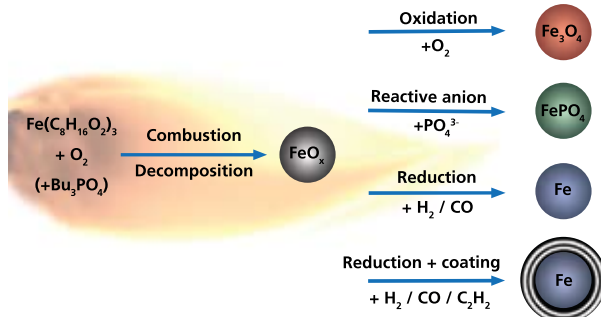


Figure 2. Depending on the metal loading the flames during the production of inorganic nanoparticles show different colors. Illustrated in this example is the combustion of metalorganic precursors containing copper, strontium, cerium and bismuth (from left to right).

Expansion to Salts and Metals: A Quantum Leap

By studying the chemical problems of the synthesis of complex inorganic materials in flame reactors, the range of accessible products can be successfully extended from oxides to most inorganic salts¹⁴ (see **Scheme 1**). Loher et al. demonstrated the use of a flame as a chemical reactor and that chemical reactions, usually performed in solid-state, can be adapted for the flame synthesis of nanoparticles. As a result of these advances, a number

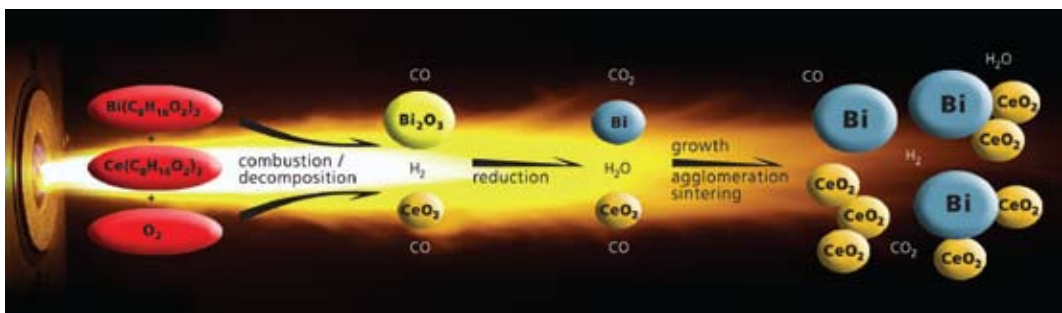
of everyday materials have become available in the form of nanoparticles, examples include: nano-gypsum,¹⁵ nano-salt¹⁶ and nano-tricalcium phosphate (**Aldrich Prod. No. 693898**).^{14,17,18} The latter has been incorporated in a number of biomedical materials and first *in vivo* tests demonstrated their successful application as biomaterials.¹⁸ A recent, preclinical study has demonstrated the advantageous re-mineralization properties of nanobioactive glass for damaged dentin (tooth repair).¹⁹



Scheme 1. Schematic illustration of the flexibility of flame spray synthesis is illustrated in this sketch. Depending on the process parameters, it is possible to produce oxide (oxidizing atmosphere), salt (addition of a reactive anion to the precursor solution), metal (oxygen starving conditions) or carbon-coated metal nanoparticles (introduction of acetylene).

Very recently, the concept of chemical aerosol engineering in flames has been extended to the synthesis of metal nanoparticles. The requirement of oxygen for combustion naturally led to production setups under oxidizing atmospheres. This circumstance, of course, impedes the synthesis of reduced materials, such as metal nanoparticles, as these would immediately react with oxygen, water or CO_2 in the flame atmosphere, forming metal oxides. To circumvent this instant oxidation of the metal nanoparticles, Grass et al. performed flame spray synthesis of a metal containing organic precursor in an oxygen-free, reducing atmosphere (**See Scheme 2**).^{20,21} This resulted in complete combustion of all oxygen present and the formation of metallic nanoparticles in the flame atmosphere.

Recently, a further synthetic step was taken to achieve controlled deposition of carbon on the metal surface of nanoparticles.²² In principle, the degree and rate of carbon deposition depends on temperature, gas composition and the metal surface. Controlled temperature profiles in the exit stream of flame reactors and additional feeding of hydrogen, carbon mono- or dioxide, methane or even acetylene provides an option to coat metals *in situ* with a carbon layer. Such core/shell metal/carbon materials, for example, can yield unexpected bulk properties. The suitability of 1 nm carbon-coated copper particles for temperature or pressure sensing was recently demonstrated. The same material dispersed in water has been proven for use in highly sensitive humidity sensor coatings.²³



Scheme 2. Reducing flame synthesis for the manufacture of metal/ceramic nanocomposite particles consisting of bismuth/ceria. The atmosphere of the flame (CO , H_2 , H_2O , CO_2 , N_2) is responsible for the reduction of bismuth oxide to metallic bismuth, but is not capable of reducing cerium oxide to metallic cerium (difference in reduction potential of bismuth and cerium).

Application Example: Self-Sterilizing Polymer Surfaces

One descriptive example of the flame spray technology is the development of highly active self-sterilizing polymer films. With this technology, it is possible to homogeneously deposit 1-2 nm scale silver nanoparticles on the surface of tricalcium phosphate carrier nanoparticles.²⁴ These metal-salt composite nanoparticles can be incorporated into a plastic film (see **Figure 3**). Such a film containing the composite nanoparticles was shown to be up to 1000 times more efficient as a killer of bacteria such as *Escherichia coli*, when compared to conventional silver preparations. One decisive factor appears to be that bacteria use the calcium carrier for their metabolism. The calcium phosphate particles, 20 to 50 nanometer in size, are absorbed by the micro-organisms and the subsequent dissolution of the calcium phosphate releases thousands of silver nanoparticles which are lethal to many bacteria. The synthesis of such complex composite materials without substantial changes in process design signifies the power of flame spray synthesis.

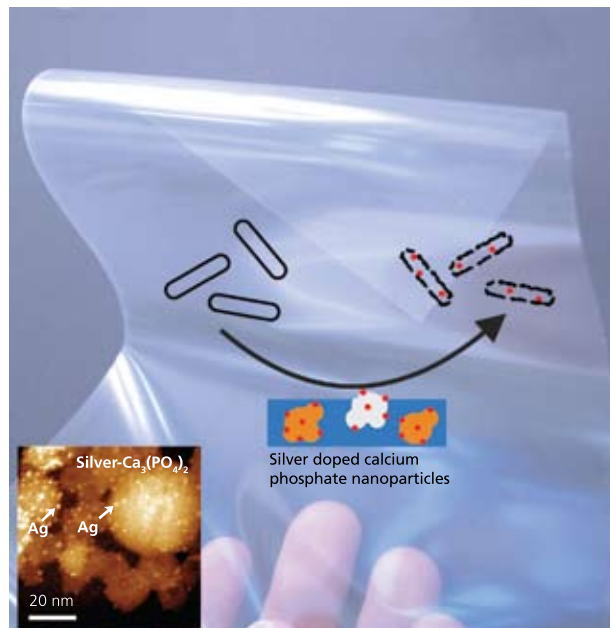


Figure 3. Composite nanoparticles with 1-2 nm silver nanoparticles homogeneously distributed on calcium phosphate carrier nanoparticles. Due to the small size and distribution on the surface of salt nanoparticles, these nanocomposites are up to 1000 times more efficient bacteria killers than conventional silver preparations.





In summary, flame spray synthesis allows the scalable fabrication of many mixed oxide, salt, metal, carbon-coated metal, silica-coated metal oxide or even metal-ceramic composite nanoparticles.²⁵ The synthesis is based on metal loaded liquid precursors and achieves accurate control over the composition and size of the nanoparticles. High batch-to-batch reproducibility, a highly homogeneous product and a wide product variety are only a few of the useful attributes of flame spray synthesis. With this technology, there are manifold opportunities to take the developed technologies to industrial products.

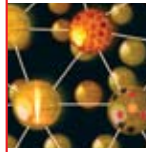
References:

- (1) Haruta, M.; Kobayashi, T.; Sano, H.; Yamada, N. *Chem. Lett.*, **1987**, 405.
- (2) Osterwalder, N.; Capello, C.; Hungerbuhler, K.; Stark, W.J. *J. Nanopart. Res.*, **2006**, 8, 1.
- (3) Zachariah, M.R.; Huzarewicz, S. *Combust. Flame*, **1991**, 87, 100.
- (4) Matsukas, T.; Friedlander, S.K. *J. Colloid Interface Sci.*, **1991**, 146, 495.
- (5) Mueller, R.; Jossen, R.; Kammler, H.K.; Pratsinis, S.E. *Aiche J.*, **2004**, 50, 3085.
- (6) Tani, T.; Watanabe, N.; Takatori, K. *J. Nanopart. Res.*, **2003**, 5, 39.
- (7) Marchal, J.; John, T.; Baranwal, R.; Hinklin, T.; Laine, R.M. *Chem. Mat.*, **2004**, 16, 822.
- (8) Stark, W.J.; Wegner, K.; Pratsinis, S.E.; Baiker, A. *J. Catal.*, **2001**, 197, 182.
- (9) Stark, W.J.; Grunwaldt, J.D.; Maciejewski, M.; Pratsinis, S.E.; Baiker, A. *Chem. Mat.*, **2005**, 17, 3352.
- (10) Stark, W.J.; Kammler, H.K.; Strobel, R.; Gunther, D.; Baiker, A.; Pratsinis, S.E. *Ind. Eng. Chem. Res.*, **2002**, 41, 4921.
- (11) Stark, W.J.; Pratsinis, S.E.; Baiker, A. *J. Catal.*, **2001**, 203, 516.
- (12) Strobel, R.; Stark, W.J.; Madler, L.; Pratsinis, S.E.; Baiker, A. *J. Catal.*, **2003**, 213, 296.
- (13) Athanassiou, E.K.; Mensing, C.; Stark, W.J. *Sens. Actuator A-Phys.*, **2007**, 138, 120.
- (14) Loher, S.; Stark, W.J.; Maciejewski, M.; Baiker, A.; Pratsinis, S.E.; Reichardt, D.; Maspero, F.; Krumeich, F.; Gunther, D. *Chem. Mat.*, **2005**, 17, 36.
- (15) Osterwalder, N.; Loher, S.; Grass, R.N.; Brunner, T.J.; Limbach, L.K.; Halim, S.C.; Stark, W.J. *J. Nanopart. Res.*, **2007**, 9, 275.
- (16) Grass, R.N.; Stark, W.J. *Chem. Commun.*, **2005**, 1767.
- (17) Brunner, T.J.; Grass, R.N.; Bohner, M.; Stark, W.J. *J. Mater. Chem.*, **2007**, 17, 4072.
- (18) Schneider, O.D.; Loher, S.; Brunner, T.J.; Uebersax, L.; Simonet, M.; Grass, R.N.; Merkle, H.P.; Stark, W.J. *J. Biomed. Mater. Res. Part B*, **2008**, 84B, 350.
- (19) Vollenweider, M.; Brunner, T.J.; Knecht, S.; Grass, R.N.; Zehnder, M.; Imfeld, T.; Stark, W.J. *Acta Biomater.*, **2007**, 3, 936.
- (20) Athanassiou, E.K.; Grass, R.N.; Stark, W.J. *Nanotechnology*, **2006**, 17, 1668.
- (21) Grass, R.N.; Stark, W.J. *J. Nanopart. Res.*, **2006**, 8, 729.
- (22) Athanassiou, E.K.; Grass, R.N.; Osterwalder, N.; Stark, W.J. *Chem. Mat.*, **2007**, 19, 4847.
- (23) Luechinger, N.A.; Loher, S.; Athanassiou, E.K.; Grass, R.N.; Stark, W.J. *Langmuir*, **2007**, 23, 3473.
- (24) Loher, S.; Schneider, O.D.; Maienfisch, T.; Bokornym, S.; Stark, W.J. *Small*, **2008**, 4, 824.
- (25) Teleki, A.; Akhtar, M.K.; Pratsinis, S.E. *J. Mater. Chem.*, **2008**, 18, 3547.

Nanoparticles—Prepared by Nanospray Combustion Process

For noble-metal nanoparticles, see page 11. For magnetic nanoparticles, see page 17.

Metallic Element Z: Symbol	Name	Composition	Form	Particle Size (nm)	Cat. No.
3: Li	Lithium titanate, spinel, nanopowder, >99%	$\text{Li}_4\text{Ti}_5\text{O}_{12}$	-	<100 (TEM) <100 (BET)	702277-25G
12: Mg	Magnesium oxide	MgO	nanopowder	<50 (BET) <25 (XRD)	549649-5G 549649-25G
12: Mg	Magnesium aluminate, spinel	$\text{MgO}\cdot\text{Al}_2\text{O}_3$	nanopowder	<50 (BET)	677396-5G
14: Si	Silicon dioxide, alumina doped, 99.99% trace metals basis	$(\text{SiO}_2)_x(\text{Al}_2\text{O}_3)_y$, aluminum 7.5 wt. %	nanoparticles, 20 wt. % in H_2O	<50	701491-25ML 701491-100ML
20: Ca	Calcium oxide, 98%	CaO	nanopowder	<160 (BET)	634182-25G 634182-100G
20: Ca	Hydroxyapatite, 97+%	$[\text{Ca}_5(\text{OH})(\text{PO}_4)_3]_x$	solid nanopowder	<200 (BET)	677418-5G 677418-10G
20: Ca	Hydroxyapatite	$[\text{Ca}_5(\text{OH})(\text{PO}_4)_3]_x$	solid nanopowder	<200 (BET)	693863-5G
20: Ca	Hydroxyapatite	$[\text{Ca}_5(\text{OH})(\text{PO}_4)_3]_x$	nanoparticles, 10 wt. % in H_2O	<200 (TEM)	702153-25ML
20: Ca	Calcium phosphate, amorphous	$\text{Ca}_2\text{O}_7\text{P}_2 \cdot \text{H}_2\text{O}$, $\text{Ca}/\text{P} \sim 1/1$	nanopowder	<150 (BET)	693871-5G
20: Ca	Tricalcium phosphate hydrate	$\text{Ca}_3(\text{PO}_4)_2 \cdot x\text{H}_2\text{O}$	nanopowder	<100 (TEM) <200 (BET)	693898-5G
22: Ti	Titanium silicon oxide, 99.8% trace metals basis	$(\text{SiO}_2)(\text{TiO}_2)$	nanopowder	<50 (BET)	641731-10G 641731-50G
22: Ti	Titanium(IV) oxide, 97+%	TiO_2	nanopowder	<100 (BET)	677469-5G
26: Fe	Iron-nickel alloy, ≥97%	Fe:Ni 55±5%:45±5%	nanopowder	<100 (BET)	677426-5G
28: Ni	Nickel cobalt oxide, 99% trace metals basis	NiO CoO	nanopowder	<150 (BET)	634360-25G 634360-100G
28: Ni	Nickel zinc iron oxide, 99+% trace metals basis	$\text{NiZnFe}_3\text{O}_4$	nanopowder	<100 (BET)	641669-10G 641669-50G
29: Cu	Copper zinc iron oxide, 98.5% trace metals basis	$\text{CuZnFe}_3\text{O}_4$	nanopowder	<100 (BET)	641650-10G 641650-50G
29: Cu	Copper iron oxide, 98.5% trace metals basis	CuFe_2O_4	nanopowder	<100 (BET)	641723-10G 641723-50G
30: Zn	Zinc iron oxide, >99% trace metals basis	ZnFe_2O_4	nanopowder	<100 (BET)	633844-10G 633844-50G
30: Zn	Zinc oxide, >97%	ZnO	nanopowder	<50 (BET)	677450-5G
39: Y	Yttrium iron oxide, 99.9% trace metals basis	$\text{Y}_3\text{Fe}_5\text{O}_{12}$	nanopowder	<100 (BET) <50 (XRD)	634417-10G



Metallic Element Z: Symbol	Name	Composition	Form	Particle Size (nm)	Cat. No.
40: Zr	Zirconium(IV) oxide-yttria stabilized	ZrO ₂	nano powder	<100 (BET)	544779-5G 544779-25G
40: Zr	Zirconium(IV) silicate, 98.5% trace metals basis	ZrSiO ₄	nano powder	<100 (BET) <50 (XRD)	634395-25G 634395-100G
40: Zr	Zirconium(IV) oxide, dispersion	ZrO ₂	nano particles, 5 wt. % in H ₂ O	<100 (BET)	643122-100ML 643122-500ML
40: Zr	Zirconium(IV) oxide, dispersion	ZrO ₂	nano particles, 10 wt. % in H ₂ O	<100 (BET)	643025-100ML 643025-500ML
47: Ag	Silver-copper alloy	CuAg ₂₅ , Ag ~ 97.5% Cu ~ 2.5%	nano powder	<100	576824-5G
47: Ag	Silver-tin alloy, 3.5% Ag basis ≥97%	AgSn ₂₅	nano powder	<150	677434-5G
50: Sn	Tin(IV) oxide	SnO ₂	nano powder	<100 (BET)	549657-5G 549657-25G
56: Ba	Barium ferrite, 99.5% trace metals basis	BaFe ₁₂ O ₁₉	nano powder	<100 (BET)	637602-25G
58: Ce	Cerium(IV)-zirconium(IV) oxide, 99.0% trace metals basis	(CeO ₂) _x (ZrO ₂) _y	nano powder	<50 (BET)	634174-25G 634174-100G
58: Ce	Aluminum cerium oxide, 99% trace metals basis	AlCeO ₃	nano powder	<50 (BET)	637866-10G 637866-50G
58: Ce	Cerium(IV) oxide, dispersion	CeO ₂	nano particles, 10 wt. % in H ₂ O	<25	643009-100ML 643009-250ML
62: Sm	Samarium strontium cobalt oxide, 99.9%	Sm _{0.5} Sr _{0.5} Co ₂ O _x	nano powder	<50 (BET)	677442-5G

Selected Nanoparticles

For a complete list of nanocomposites please visit sigma-aldrich.com/nanocomposites

Metallic Element Z: Symbol	Name	Composition	Form	Particle Size (nm)	Cat. No.
6: C	Carbon, ≥99% trace metals basis	C	nano powder	<50 (BET)	633100-25G 633100-100G
6: C	Diamond, ≥97% trace metals basis	C	nano powder	<10 (BET)	636428-1G 636428-5G
6: C	Diamond, ≥95% trace metals basis	C	nano powder	<10 (BET)	636444-1G 636444-5G
22: Ti	Titanium(IV) oxide, mixture of rutile and anatase, 99.9% trace metals basis	TiO ₂	nano particles paste, 53-57 wt. % in diethylene glycol monobutyl ether/ethylene glycol	<250 (DLS) ~21 (primary particle size of starting nanopowder)	700355-25G
22: Ti	Titanium(IV) oxide, mixture of rutile and anatase, 99.9% trace metals basis	TiO ₂	nano particles, 33-37 wt. % in H ₂ O	~21 (primary particle size of starting nanopowder) <150 (DLS)	700347-25G 700347-100G
22: Ti	Titanium(IV) oxide, mixture of rutile and anatase, 99.9% trace metals basis	TiO ₂	nano particles, 45-47 wt. % in xylene	~15 (primary particle size of starting nanopowder) <100 (DLS)	700339-100G
13: Al	Aluminum oxide, dispersion	Al ₂ O ₃	nano particles, 20 wt. % in isopropanol	<50 (DLS)	702129-100G 702129-500G
49: In	Indium tin oxide, dispersion	In ₂ O ₃ 90% SnO ₂ 10%	30 wt. % in isopropanol	<100 (DLS)	700460-25G 700460-100G
39: Y	Yttrium(III) oxide, dispersion, ≥99.9% trace metals basis	Y ₂ O ₃	nano particles, 10 wt. % in isopropanol	<100 (DLS)	702048-100G
58: Ce	Cerium(IV) oxide, >99.95% trace metals basis	CeO ₂	nano powder	<50 (BET)	700290-25G 700290-100G



General Metal Precursors

For noble metal precursors, see page [11](#). For magnetic metal precursors, see page [17](#).

Metallic Element Z: Symbol	Name	Structure	Cat. No.
12: Mg	Magnesium acetylacetone dihydrate, 98%		129577-25G
12: Mg	Magnesium acetate tetrahydrate, 99.999% trace metals basis		229768-10G 229768-100G
13: Al	Aluminum-tri-sec-butoxide, 97%		201073-5G 201073-100G 201073-500G
13: Al	Aluminum ethoxide, 97%		235857-5G 235857-25G 235857-100G
13: Al	Aluminum <i>tert</i> -butoxide		235849-10G 235849-50G
13: Al	Aluminum isopropoxide, 99.99+% trace metals basis		229407-10G 229407-50G 229407-250G
14: Si	Hexamethyldisiloxane, ≥98%		205389-5ML 205389-100ML 205389-500ML
14: Si	Tetraethyl orthosilicate, 99.999% trace metals basis		333859-25ML 333859-100ML
14: Si	Trimethoxymethylsilane, 98+%		679232-50G
14: Si	Triethoxy(octyl)silane, ≥98% 99.99% trace metals basis		679305-50G
20: Ca	Calcium 2-ethylhexanoate, 98%		362964-5G 362964-25G
22: Ti	Titanium(IV) methoxide, 99.99+% trace metals basis		463582-25G
22: Ti	Titanium(IV) ethoxide		244759-50G 244759-250G
22: Ti	Titanium(IV) propoxide, 98%		253081-100G 253081-500G
22: Ti	Titanium(IV) isopropoxide, 99.999% trace metals basis		377996-5ML 377996-25ML 377996-100ML
22: Ti	Titanium(IV) butoxide, 97%		244112-5G 244112-100G 244112-500G 244112-2KG
22: Ti	Titanium(IV) <i>tert</i> -butoxide		462551-25ML 462551-50ML
22: Ti	Titanium(IV) oxide acetylacetone		330833-10G 330833-50G
29: Cu	Copper(II) nitrate hydrate, 99.999% trace metals basis		229636-5G 229636-25G 229636-100G
29: Cu	Copper(II) acetate, 99.999% trace metals basis		517453-5G 517453-25G



Metallic Element Z: Symbol	Name	Structure	Cat. No.
29: Cu	Copper(II) 2-ethylhexanoate		337323-5G 337323-25G
30: Zn	Zinc nitrate hydrate, 99.999% trace metals basis	$\text{Zn}(\text{NO}_3)_2 \cdot 6\text{H}_2\text{O}$	230006-25G 230006-250G
30: Zn	Zinc acetate dihydrate, 99.999% trace metals basis		379786-5G 379786-25G
30: Zn	Zinc acetylacetone hydrate, 99.995% trace metals basis		480991-5G 480991-25G
38: Sr	Strontium acetylacetone hydrate		704512-5G 704512-25G
39: Y	Yttrium(III) 2-ethylhexanoate, 99.9% trace metals basis		347086-10G 347086-50G
40: Zr	Zirconium(IV) ethoxide, 97%		339121-5G 339121-25G
40: Zr	Zirconium(IV) propoxide solution		333972-100ML 333972-500ML
40: Zr	Zirconium(IV) <i>tert</i> -butoxide, 99.999% trace metals basis		560030-5G 560030-25G
40: Zr	Zirconium(IV) acetylacetone, 98%		338001-25G 338001-100G
50: Sn	Tributyltin methoxide, 97%		229245-25G 229245-100G
50: Sn	Tin(IV) <i>tert</i> -butoxide, 99.99+% trace metals basis		494135-5G 494135-25G
50: Sn	Tin(II) acetylacetone, 99%		697478-5G
50: Sn	Tin(II) 2-ethylhexanoate, ~95%		S3252-100G S3252-250G S3252-500G S3252-1KG
56: Ba	Barium 2-ethylhexanoate, 98%		361704-5G
56: Ba	Barium acetate, 99.999% trace metals basis		255912-10G 255912-50G
72: Hf	Hafnium isopropoxide isopropanol adduct, 99.9% trace metals basis		697508-5G
75: Re	Dirhenium decacarbonyl, 98%	$\text{Re}_2(\text{CO})_{10}$	245003-500MG 245003-5G



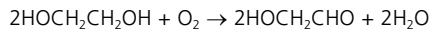
Majiong Jiang,¹ Claire M. Cobley,²
Dr. Byungkwon Lim² and Prof. Younan Xia^{2*}
¹Department of Chemistry and ²Department
of Biomedical Engineering, Washington
University, St. Louis, MO
*Email: xia@biomed.wustl.edu

Introduction

Noble-metal nanostructures are widely used in a variety of applications ranging from catalysis to electronics, surface plasmon resonance (SPR), surface-enhanced Raman scattering (SERS), and biomedical research.^{1–3} Different applications demand nanostructures with specific morphologies. For example, catalysis often requires the noble-metal nanostructures to be dispersed on ceramic supports with high surface areas, while nanowires are needed for transport measurements and as interconnects in electronic devices. Morphology may also provide a sensitive parameter for enhancing and/or tailoring the properties of noble-metal nanostructures. It has been established that the catalytic activity and selectivity of noble-metal nanoparticles are strongly dependent on the facets exposed on the surface. For Pt, its activity for the oxygen reduction reaction (ORR) increases in the order of (100) < (111) < (110) in a non-adsorbing electrolyte.⁴ In the case of Pd, its (100) facets are almost four times more reactive than the (111) facets for formic acid oxidation.⁵ On the other hand, the morphology of Au or Ag nanostructures not only determine SPR characteristics, but also the merits in SERS detection.⁶ Therefore, controlling the morphologies of noble-metal nanostructures is crucial to enhancing their performance in various applications.

Polyol Synthesis of Nanostructures

The polyol process has become a popular method for preparing noble-metal nanostructures with well-defined morphologies. The primary step in this process involves heating a polyol such as ethylene glycol (EG) (**Aldrich Prod. No. 324558**) with a metal salt (i.e., a precursor to the noble metal) in the presence of a polymeric capping agent such as poly(vinylpyrrolidone) (PVP) (**Aldrich Prod. Nos. 234257, 856568, 437190**) to generate metal atoms. Upon heating EG to the temperature range of 140–160 °C, glycolaldehyde (**Aldrich Prod. No. G6805**) (the reducing agent) is produced through the following oxidation reaction:⁷



The ability of polyols to dissolve many metal salts and their temperature-dependent reducing power makes polyol synthesis an attractive route to nanostructures of various noble metals including Ag, Au, Pd, Pt, Rh, Ru, and Ir.

Control of Nanostructure Morphology

In solution-phase synthesis of noble-metal nanostructures, the final morphology is primarily determined by the twin structure of seeds and the growth rates of different crystallographic facets. In the early stage of a reaction, a precursor compound is either decomposed or reduced to generate zero-valent atoms, which can form a cluster with fluctuating structure also known as a nucleus. Once the cluster has grown past a critical size, structural fluctuations become so energetically costly that it will be locked into a well-defined structure and become a seed. As illustrated in **Figure 1**, the seed serves as a bridge between atoms and the nanostructure, and it may take a single-crystal or multiply twinned structure.⁸ In practice, the twin structure of seeds can be controlled by manipulating the reduction kinetics. When the reduction rate is relatively fast, thermodynamically favorable species such as single-crystal and multiply twinned seeds are dominant in the nucleation stage. The former can evolve into octahedrons or cubes, while the latter into decahedrons or pentagonal nanowires depending on the reaction conditions. When the reduction rate is considerably slowed down, the reaction will become kinetically controlled. In this case, plate-like seeds with planar defects such as stacking faults can form at the initial nucleation stage, which then evolve into hexagonal and triangular nanoplates that deviate from the thermodynamically favored morphologies. The distribution of differently twinned seeds can be further altered by selectively employing or blocking oxidative etching, in which zero-valent metal atoms are oxidized back to ions. In one case, the twinned seeds can be selectively removed by the O₂/Cl⁻ etchant, leaving behind single-crystal seeds in the reaction solution.⁹ In most cases, the introduction of selective capping agents provides a powerful means of controlling the relative growth rates of different crystallographic facets as they can interact strongly with specific facets and thus change the relative free energies for different facets. This kind of chemisorption or surface capping has a profound impact on the final morphology of metal nanostructures. For instance, PVP is a polymeric capping agent whose oxygen atoms bind most strongly to the {100} facets of Ag and thus facilitate the formation of Ag nanowires or nanocubes.^{10,11}

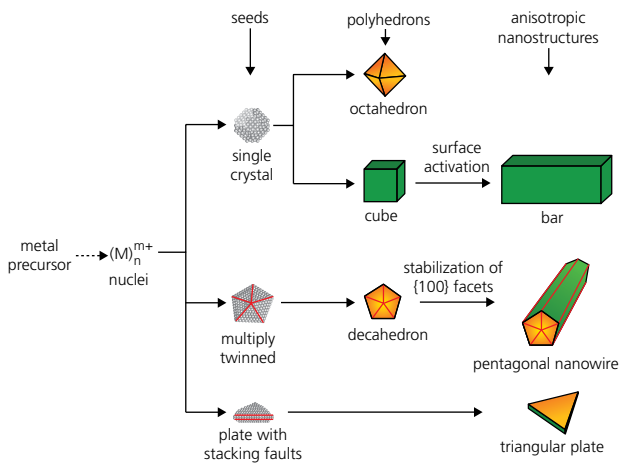


Figure 1. Schematic illustration of the reaction pathways that lead to face-centered cubic metal nanostructures with different morphologies. First, a precursor is reduced or decomposed to form the nuclei (small clusters). Once the nuclei have grown past a certain size, they become seeds with a single-crystal or multiply twinned structure. If stacking faults are introduced, plate like seeds will be formed. The green and orange colors represent the {100} and {111} facets, respectively. Twin planes are depicted with red lines. Reprinted from Ref. 8 with permission from Wiley-VCH.

Case Study I: Silver (Ag)

Silver nanostructures are probably best known for their morphology-dependent optical properties like SPR.¹¹ They also serve as the most popular substrates for SERS and the most selective catalyst for epoxidation of ethylene. Uniform Ag nanowires can be produced by adding CuCl_2 (**Aldrich Prod. No. 203149**) to a typical polyol reduction of AgNO_3 (**Aldrich Prod. No. 204390**) with EG (**Figure 2a**).¹² The Cu(II) ions will be reduced by EG into Cu(I). Both the Cu(I) and Cl⁻ ions play important roles. Copper ions promote the growth of wires by reducing the amount of oxygen on the surface, preventing the multiply twinned seeds from being dissolved due to oxidative etching and unblocking sites for further deposition of Ag atoms. Ethylene glycol can recycle Cu(II) back to Cu(I), so only a small amount of Cu(II) ions needs to be added to scavenge the adsorbed oxygen on the metal surface. Chloride ions control the concentration of free Ag⁺ in the solution by forming AgCl, consequently decreasing the reduction rate and facilitating preferential growth on the high energy twin boundaries at the ends of the wire. In a typical synthesis, PVP is also required to preferentially passivate the {100} surfaces that make up the sides of the nanowires.

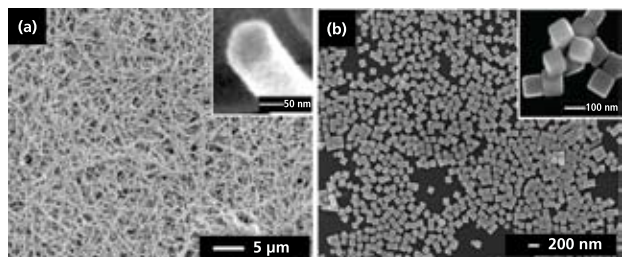


Figure 2. Silver nanostructures synthesized by the modified polyol process. (a) SEM image of Ag nanowires synthesized by the addition of CuCl_2 . Inset shows the pentagonal cross section of the nanowires. Reprinted from Ref. 12 with permission from the Royal Society of Chemistry. (b) SEM image of Ag nanocubes synthesized by the addition of NaHS. Reprinted from Ref. 27 with permission from Wiley-VCH.

Trace amounts of other ionic species are also important in the morphological control of Ag nanostructures. By adding small amounts of sulfide in the form of either Na_2S (**Aldrich Prod. No. 407410**) or NaHS (**Aldrich Prod. No. 161527**) to the polyol reduction of AgNO_3 , Ag nanocubes can be routinely produced as uniform samples and in relatively large quantities (**Figure 2b**).¹³ Since Ag_2S is a known catalyst for Ag reduction, the proposed mechanism involves small Ag_2S seeds generated immediately after the addition of AgNO_3 . These seeds catalyze the reduction and serve as sites for the growth of high quality cubes. Since the reaction is kinetically controlled, more thermodynamically favorable twinned seeds are not able to form, and the final product is dominated by single-crystal species like nanocubes. PVP again plays the role of preferentially capping the {100} faces of Ag nanocubes.

Case Study II: Gold (Au)

Gold nanostructures have received considerable attention due to their excellent chemical stability, bio-inertness, SPR/SERS properties, and unique catalytic activity. There have been many demonstrated methods for controlling the morphology of Au nanostructures.¹⁴⁻¹⁶ As for the Ag system, the selection of reducing agent, stabilizer, and reaction temperature is critical to forming a particular morphology. In most cases, strong reducing agents, as exemplified by polyol reduction, facilitate the formation of thermodynamically favored polyhedral Au nanostructures. There are, however, notable differences. For example, in contrast to the Ag system, the binding of PVP to Au does not appear to be sufficiently strong to promote the formation of {100} facets. As a result, single-crystal and multiply twinned polyhedrons enclosed by {111} facets such as octahedrons, icosahedrons, and decahedrons are dominant morphologies for Au nanostructures in the polyol synthesis.

For instance, Au octahedrons have been synthesized in high yields via a modified polyol process by using polyethylene glycol 600 (**Aldrich Prod. No. 202401**) as a reducing agent, which also serves as a solvent in the synthesis (**Figure 3a**).¹⁷ In this case, the addition of a small amount of sodium borohydride (NaBH_4) (**Aldrich Prod. No. 480886**), prior to the addition of an aqueous gold(III) chloride (AuCl_3) solution (**Aldrich Prod. No. 334049**), is the key to high-yield production of uniform Au octahedrons. It serves as a strong reducing agent and thus ensures the fast reduction of the Au precursor. On the other hand, the multiply twinned nanostructures of Au such as decahedrons can be produced at a relatively high concentration of PVP in the polyol reduction of HAuCl_4 (**Aldrich Prod. No. 484385**) with diethylene glycol (**Aldrich Prod. No. H26456**) (**Figure 3b**).¹⁸ It seems that the high concentration of PVP helps to block the surfaces of Au decahedrons from the oxidative etching by O_2/Cl^- pair. As a result, these twinned nanostructures could be stabilized and accumulate throughout the reaction.

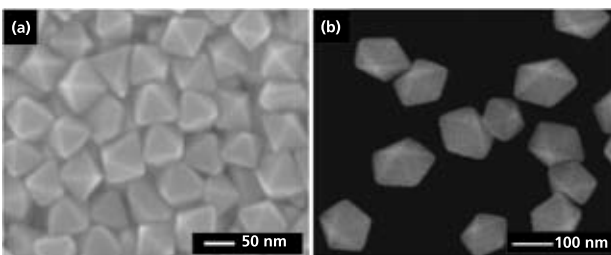


Figure 3. Gold nanostructures synthesized by the modified polyol process. (a) SEM image of Au octahedrons made by the addition of a small amount of NaBH_4 in a polyol reduction of AuCl_3 with polyethylene glycol 600. Reprinted from Ref. 17 with permission from Wiley-VCH. (b) SEM image of Au decahedrons obtained by a polyol reduction of HAuCl_4 with diethylene glycol in the presence of a high concentration of PVP. Reprinted from Ref. 18 with permission from the American Chemical Society.

Case Study III: Palladium (Pd)

Palladium is a key catalyst for a variety of reactions including hydrogenation, dehydrogenation, and carbon-carbon bond-forming processes such as Suzuki, Heck, or Stille coupling. In general, the predominant morphology of Pd nanostructures in a typical polyol reduction of Na_2PdCl_4 (**Aldrich Prod. No. 379808**) with EG is the truncated octahedron.¹⁹ Morphological control of Pd nanostructures can be achieved by introducing specific capping agents such as Br⁻ ions and/or by employing oxidative etching. In one example, Pd nanobars with a rectangular cross-section can be synthesized by adding Br⁻ ions to the polyol



reduction of Na_2PdCl_4 .²⁰ Bromide ions bind strongly to the {100} facets of Pd, resulting in the formation of cubic Pd seeds in the nucleation stage. The formation of Pd nanobars can be attributed to anisotropic growth of the cubic seeds driven by a selective activation process, which involves the localized oxidative etching on one of the six faces of the cubic seed to remove some of the Br ions. This facilitates preferential growth of the cubic seed along one direction and eventually leads to the formation of Pd nanobars enclosed by the {100} facets (**Figure 4a**).

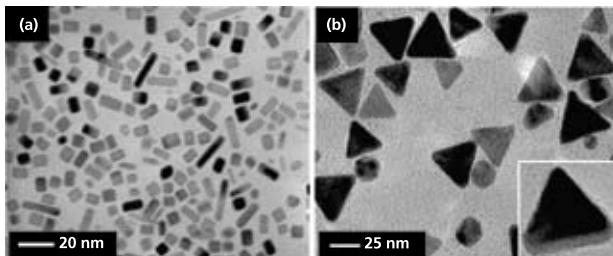


Figure 4. Palladium nanostructures synthesized by the modified polyol process. (a) TEM image of Pd nanobars synthesized by the addition of KBr in a polyol reduction of Na_2PdCl_4 with EG in the presence of a small amount of water as a co-solvent. Reprinted from Ref. 20 with permission from the American Chemical Society. (b) TEM image of triangular Pd nanoplates synthesized by introducing a small amount of FeCl_3 and HCl into a polyol reduction of Na_2PdCl_4 with EG. Reprinted from Ref. 21 with permission from the American Chemical Society.

As another demonstration, Pd triangular nanoplates have been synthesized by introducing Fe(III) species into the polyol synthesis (**Figure 4b**).²¹ The reduction rate is substantially slowed down due to the presence of two wet etchants for Pd(0), i.e., Fe(III) species and the O_2/Cl^- pair. The oxidative etching can be further enhanced by adding an acid to lower the pH of the reaction solution. This kinetically controlled process under the slow reduction rate enables the formation of plate-like seeds in the nucleation stage, which then gradually evolve into triangular nanoplates via preferential addition of newly formed Pd atoms to the side faces of developing nanoplates. These nanoplates of Pd exhibit SPR peaks in the visible region due to their increased sizes. Thanks to the sharp corners and edges, they could serve as active substrates for SERS.

Case Study IV: Platinum (Pt)

Platinum is an invaluable catalyst for a variety of industrial applications, such as hydrogenation, oil cracking, and CO/NO_x oxidation in catalytic converters. It also serves as the most effective electrocatalyst for both ORR and fuel oxidation in the operation of a fuel cell.^{22,23} For most of these applications, it is critical to disperse Pt nanostructures on solid supports. The polyol reduction can be modified to grow Pt nanowires on various substrates by adding a small amount of Fe(II) or Fe(III). In a typical process, Pt(II) species are formed by reducing H_2PtCl_6 (**Aldrich Prod. No. 262587**) with EG at 110 °C in the presence of PVP. By adding a trace amount of FeCl_3 (**Aldrich Prod. No. 451649**) as an oxidative etchant for Pt(0), the nucleation of Pt atoms can be controlled to grow into uniform nanowires directly on a Pt or W gauze (**Figure 5a**).²³ The Pt gauze (**Aldrich Prod. Nos. 298107, 298093**) covered with Pt nanowires showed enhanced activity, over 1.5 times higher than that of the Pt/C (E-TEK) catalyst, towards the methanol oxidation reaction. In addition, Pt nanowires can also be readily grown on other substrates such as electrospun TiO_2 nanofibers and patterned silicon substrates using this simple approach.^{24,25}

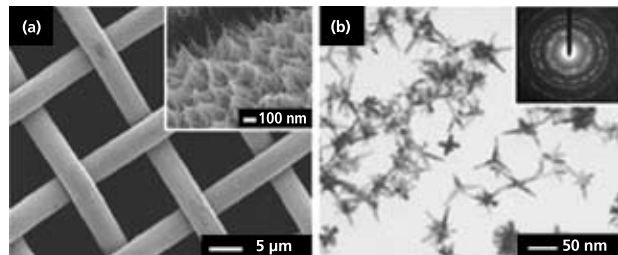


Figure 5. Platinum nanostructures synthesized by the modified polyol process. (a) SEM image of Pt nanowires on Pt gauze. Inset shows the edge view of the Pt nanowires growing outward from the surface of the gauze. Reprinted from Ref. 23 with permission from the American Chemical Society. (b) TEM image of Pt multipods synthesized through an iron-mediated polyol process. In this case, the kinetics of polyol reduction is controlled by abruptly blocking oxidative etching with N_2 flow, which initiates overgrowth of Pt seeds into highly branched nanostructures. Reprinted from Ref. 26 with permission from Wiley-VCH.

In the absence of substrates, highly branched nanostructures of Pt can be produced through a similar mechanism.²⁶ The key to the formation of branched nanostructures is to abruptly block oxidative etching by flowing N_2 (**Aldrich Prod. No. 295574**) and thus removing O_2 in the reaction system. In this case, the concentration of Pt atoms dramatically increases to a high level, leading to overgrowth of the seeds into highly branched nanostructures such as multipods (**Figure 5b**).

Conclusion

We have demonstrated that synthesis of noble-metal nanostructures with various morphologies can be achieved by the polyol method. Although the exact mechanisms related to the formation of particular morphologies are yet to be fully understood, it has been proven that some of the important reaction parameters such as reduction kinetics, oxidative etching, and surface capping could be combined to provide an effective route to maneuver both the twin structure of seeds and the facets of the seed surface, the two key factors in determining the final morphology of the noble-metal nanostructure. Further improvement in this research area will be possible as our understanding of the nucleation and growth mechanisms is advanced. The ability to control the morphology of noble-metal nanostructures provides a great opportunity to realize a variety of fascinating morphology-dictated properties and applications.

References:

- (1) Trimm, D. L.; Onsan, Z. I. *Catal. Rev.*, **2001**, *43*, 31. (2) Wiley, B.; Sun, Y.; Xia, Y. *Acc. Chem. Res.*, **2007**, *40*, 1067. (3) Skrabalak, S. E.; Chen, J.; Au, L.; Lu, X.; Li, X.; Xia, Y. *Adv. Mater.*, **2007**, *19*, 3177. (4) Stamenkovic, V. R.; Fowler, B.; Mun, B. S.; Wang, G.; Ross, P. N.; Lucas, C. A.; Markovic, N. M. *Science*, **2007**, *315*, 493. (5) Habas, S. E.; Lee, H.; Radmilovic, V.; Somorjai, G. A.; Yang, P. *Nat. Mater.*, **2007**, *6*, 692. (6) McLellan, J. M.; Li, Z.-Y.; Siekkinen, A. R.; Xia, Y. *Nano Lett.*, **2007**, *7*, 1013. (7) Skrabalak, S. E.; Wiley, B. J.; Kim, M.; Formo, E. V.; Xia, Y. *Nano Lett.*, **2008**, *8*, 2077. (8) Xia, Y.; Xiong, Y.; Lim, B.; Skrabalak, S. E. *Angew. Chem. Int. Ed.*, **2009**, *48*, 60. (9) Wiley, B.; Herricks, T.; Sun, Y.; Xia, Y. *Nano Lett.*, **2004**, *4*, 1733. (10) Wiley, B.; Sun, Y.; Xia, Y. *Langmuir*, **2005**, *21*, 8077. (10) Sun, Y.; Xia, Y. *Science*, **2002**, *298*, 2176. (11) Wiley, B.; Im, S. H.; Li, Z.-Y.; McLellan, J.; Siekkinen, A.; Xia, Y. *J. Phys. Chem. B*, **2006**, *110*, 15666. (12) Korte, K. E.; Skrabalak, S. E.; Xia, Y. *J. Mater. Chem.*, **2008**, *18*, 437. (13) Siekkinen, A. R.; McLellan, J. M.; Chen, J.; Xia, Y. *Chem. Phys. Lett.*, **2006**, *432*, 491. (14) Lim, B.; Camargo, P. H. C.; Xia, Y. *Langmuir*, **2008**, *24*, 10437. (15) Lu, X.; Yavuz, M. S.; Tuan, H.-Y.; Korgel, B. A.; Xia, Y. *J. Am. Chem. Soc.*, **2008**, *130*, 8900. (16) Lu, X.; Tuan, T.-Y.; Korgel, B. A.; Xia, Y. *Chem. Eur. J.*, **2008**, *14*, 1584. (17) Li, C.; Shuford, K. L.; Park, Q.-H.; Cai, W.; Li, Y.; Lee, E. J.; Cho, S. O. *Angew. Chem. Int. Ed.*, **2007**, *46*, 3264. (18) Seo, D.; Yoo, C. I.; Chung, I. S.; Park, S. M.; Ryu, S.; Song, H. *J. Phys. Chem. C*, **2008**, *112*, 2469. (19) Xiong, Y.; Chen, J.; Wiley, B.; Xia, Y. *J. Am. Chem. Soc.*, **2005**, *127*, 7332. (20) Xiong, Y.; Cai, H.; Wiley, B. J.; Wang, J.; Kim, M. J.; Xia, Y. *J. Am. Chem. Soc.*, **2007**, *129*, 3665. (21) Xiong, Y.; McLellan, J. M.; Chen, J.; Yin, Y.; Li, Z.-Y.; Xia, Y. *J. Am. Chem. Soc.*, **2005**, *127*, 17118. (22) Lim, B.; Lu, X.; Jiang, M.; Camargo, P. H. C.; Cho, E. C.; Lee, E. P.; Xia, Y. *Nano Lett.*, **2008**, *8*, 4043. (23) Lee, E. P.; Peng, Z.; Chen, W.; Chen, S.; Yang, H.; Xia, Y. *ACS Nano*, **2008**, *2*, 2167. (24) Formo, E.; Lee, E.; Campbell, D.; Xia, Y. *Nano Lett.*, **2008**, *8*, 668. (25) Lee, E. P.; Xia, Y. *Nano Res.*, **2008**, *1*, 129. (26) Chen, J.; Herricks, T.; Xia, Y. *Angew. Chem. Int. Ed.*, **2005**, *44*, 2589.

Noble Metal Nanoparticles

For general metal precursors, see page 6. For magnetic metal precursors, see page 17.

Metallic Element Z: Symbol	Name	Form	Particle Size (nm)	Cat. No.
46: Pd	Palladium, 99.9%	nanopowder	particle size <25 (TEM)	686468-500MG
47: Ag	Silver, 99% trace metals basis	nanopowder	particle size <150	484059-5G
47: Ag	Silver, 99.5% trace metals basis	nanopowder	particle size <100	576832-5G
47: Ag	Silver, dispersion	nano particles, 10 wt. % in ethylene glycol	particle size <100 (TEM)	658804-5G 658804-25G
47: Ag	Silver, dispersion	nano particles, 0.25 mM in H ₂ O	particle size ~157	675318-5ML
47: Ag	Decanethiol functionalized silver nanoparticles	solution, 0.1 % (w/v) in hexane	particle size 3 - 7 (DLS)	673633-25ML
47: Ag	Dodecanethiol functionalized silver nanoparticles	solution, 0.25 % (w/v) in hexane	particle size 5 - 15 (DLS)	667838-25ML
78: Pt	Platinum, 99.9+%	nanopowder	particle size <50 (BET)	685453-500MG
79: Au	Gold, 99.9+% trace metals basis	nanopowder	particle size <100	636347-1G
79: Au	Gold colloid	nano particles, HAuCl ₄ ~ 0.01% ~ 1 A ₅₂₀ units/mL	mean particle size 3.0 - 5.5 (monodisperse) particle size 5	G1402-25ML
79: Au	Gold colloid	nano particles, HAuCl ₄ ~ 0.01% ~ 1 A ₅₂₀ units/mL	mean particle size 8.5 - 12.0 (monodisperse) particle size 10	G1527-25ML
79: Au	Gold colloid	nano particles, HAuCl ₄ ~ 0.01% ~ 1 A ₅₂₀ units/mL	mean particle size 17 - 23 (monodisperse) particle size 20	G1652-25ML
79: Au	Octanethiol functionalized gold nanoparticles	solution, 2 % (w/v) in toluene	particle size 2 - 4 (DLS)	660426-5ML
79: Au	Dodecanethiol functionalized gold nanoparticles	solution, 2 % (w/v) in toluene	particle size 2 - 4 (DLS)	660434-5ML
79: Au	Dodecanethiol functionalized gold nanoparticles, 0.7-0.9% solid material basis	dispersion, HAuCl ₄ 0.01% in toluene	particle size 3 - 6	54349-10ML-F

Noble Metal Precursors

For general metal precursors, see page 6. For magnetic metal precursors, see page 17.

Metallic Element Z: Symbol	Name	Structure	Cat. No.
44: Ru	Triruthenium dodecacarbonyl, 99%		245011-1G 245011-5G
45: Rh	Rhodium(II) hexanoate, dimer, 97%		481173-1G
45: Rh	Rhodium(II) octanoate, dimer		442100-500MG
46: Pd	Palladium(II) acetate, 99.98% trace metals basis		379875-1G 379875-5G
46: Pd	Palladium(II) acetylacetone, 99%		209015-1G 209015-5G
46: Pd	Palladium(II) propionate, 99.9+% trace metals basis		481165-1G 481165-5G
46: Pd	Palladium(II) nitrate solution, 99.999% trace metals basis	Pd(NO ₃) ₂	380040-10ML 380040-50ML
47: Ag	Silver acetate, 99.99% trace metals basis		204374-10G 204374-50G
47: Ag	Silver acetylacetone, 98%		323489-1G 323489-5G
47: Ag	Silver nitrate, 99.9999% trace metals basis	AgNO ₃	204390-1G 204390-10G 204390-50G 204390-250G



Noble-Metal Nanostructures with Controlled Morphologies



Metallic Element Z: Symbol	Name	Structure	Cat. No.
47: Ag	Silver carbonate, 99.999% trace metals basis	Ag ₂ CO ₃	438448-1G 438448-10G
47: Ag	Silver sulfate, 99.999% trace metals basis	Ag ₂ SO ₄	204412-10G 204412-50G
76: Os	Triosmium dodecacarbonyl, 98%		249742-250MG 249742-1G
77: Ir	Iridium(III) acetylacetoneate, 97%		333352-500MG 333352-2.5G
78: Pt	Platinum(II) acetylacetoneate, 99.99% trace metals basis		523038-1G
78: Pt	Platinum(IV) chloride, 99.99+% trace metals basis	PtCl ₄	379840-250MG 379840-1G
78: Pt	Chloroplatinic acid hydrate, 99.995% trace metals basis	H ₂ PtCl ₆ • xH ₂ O	254029-250MG 254029-1G 254029-5G
78: Pt	Platinum(II) cyanide, 99.99% trace metals basis	Pt(CN) ₂	442097-500MG 442097-2.5G
79: Au	Gold(III) chloride hydrate, 99.999% trace metals basis	HAuCl ₄	254169-500MG 254169-5G
79: Au	Gold(III) chloride, 99.99+% trace metals basis	AuCl ₃	379948-250MG 379948-1G
79: Au	Potassium gold(III) chloride, 99.995% trace metals basis	K(AuCl ₄)	450235-250MG 450235-1G
79: Au	Gold(III) chloride solution, 99.99% trace metals basis	HAuCl ₄	484385-10G 484385-50G
79: Au	Gold(III) chloride trihydrate, ≥99.9% trace metals basis	HAuCl ₄ • 3H ₂ O	520918-1G 520918-5G 520918-25G

Capping Agents

For a complete list of PEGs and other hydrophilic polymers please visit sigma-aldrich.com/poly

Name	Structure	Molecular Weight	Cat. No.
Polyvinylpyrrolidone		~10,000	PVP10-100G PVP10-500G PVP10-1KG PVP10-12KG
		average M _w ~29,000	234257-5G 234257-100G 234257-500G
		~40,000	81420-100G 81420-500G 81422-1KG
		average M _w ~55,000	856568-5G 856568-100G 856568-500G 856568-12X500G
		~360,000	81440-250G 81440-1KG
		average M _w ~1,300,000 by LS	437190-25G 437190-500G 437190-1KG
Poly(ethylene glycol)		average mol wt 400	P3265-500G P3265-1KG
		average M _n 570-630	202401-5G 202401-250G 202401-500G 202401-20KG

Application Note: Synthesis of Silver Nanowires

Uniform Ag nanowires can be readily synthesized using a modified polyol process. A typical synthesis involves ethylene glycol (EG) (**Aldrich Prod. No. 324558**) as both the solvent and the reducing agent, with AgNO_3 (**Aldrich Prod. No. 204390**) and poly(vinylpyrrolidone) (PVP, MW=55000) (**Aldrich Prod. No. 856568**) as the Ag precursor and the polymeric capping agent, respectively. In this synthesis, CuCl_2 (**Aldrich Prod. No. 203149**) species can be added to facilitate the anisotropic growth of Ag nanowires. In a typical synthesis, 5 mL of EG was added to a disposable glass vial with a Teflon stir bar in it; the vial was then suspended in an oil bath (temperature = 151.5 °C) and heated for 1 h under magnetic stirring (260 rpm). At 1 h, 40 μL of a 4 mM CuCl_2 solution in EG was injected into the heated EG. The solution was heated for an additional 15 min. 1.5 mL of a 0.147 M PVP solution in EG (concentration calculated in terms of the repeating unit) was then injected into the heated EG, followed by the addition of 1.5 mL of a 0.094 M AgNO_3 solution in EG. The color of the reaction solution changed as follows: initially clear and colorless to yellow (within 1 min), to red-orange (within 3 min), to green, beginning cloudiness (within 5 min), to cloudiness, with a gradual shift from green to brown-red (within 30 min), and finally to opaque gray with wisps indicating the formation of long nanowires (within 1 to 1.5 h). Upon formation of Ag nanowires, the reaction was quenched by cooling the reaction vial in a room temperature water bath. The products were washed with acetone once and water three times to remove excess EG and PVP prior to characterization.

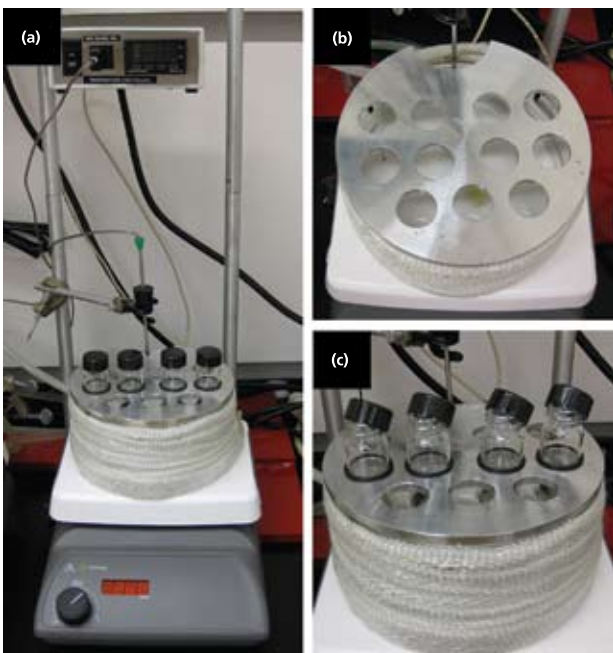


Figure 1. Experimental setup used to prepare Ag nanowires.
(a) A photograph of the entire experimental setup. A temperature-controlled stirring hotplate is used, and the reaction is performed in a disposable glass vial suspended in an oil-containing crystallization dish. (b) A photograph of the custom-made vial holder, designed to rest on top of the oil-containing crystallization dish and hold up to eleven reaction vials. (c) A close-up photograph of the reaction vials. The reaction vials are supported by an O-ring and suspended in a heated oil bath. The caps are tilted off-angle during initial preheating to allow water vapor to escape.



Application Note: Synthesis of Silver Nanowires



ALDRICH®
Chemistry

Sigma-Aldrich Offers Components for Experimental Setup

Components for Experimental Setup

	Cat. No.
IKA® RCT basic IKAMAG® safety control hot plate stirrer, AC input 115 V	Z645052
IKA RCT basic IKAMAG safety control hot plate stirrer, AC input 230 V	Z645060
IKA ETS-D5 temperature controller	Z645125
IKA support for stirring hotplate, boss head clamp, H44	Z403571
IKA support for stirring hotplate, adjustable stand support, R380	Z403601

IKA and IKAMAG are registered trademarks of IKA Works, Inc.

sigma-aldrich.com

SIGMA-ALDRICH®



Sheng Peng and Shouheng Sun*

Department of Chemistry
Brown University
Providence, Rhode Island 02912, USA

*E-mail: ssun@brown.edu

Introduction

Magnetic nanoparticles have attracted tremendous attention due to their novel properties and their potential applications in magnetic recording, magnetic energy storage and biomedicine.^{1–3} Thanks to numerous research efforts, great progress has been made on the design and fabrication of magnetic nanoparticles with controllable size, morphology, structure, composition, and magnetic properties. A variety of “bottom-up” synthesis methods have been developed and, as a result, magnetic nanoparticles are now routinely made from solution-phase thermal decomposition, metal reduction, and metal salt co-precipitation. To produce monodisperse nanoparticles with a standard deviation in diameter of less than 10%, a burst nucleation event should occur in a supersaturated solution without the formation of new nuclei and the produced nuclei would grow uniformly thereafter. Practically, a hot-injection procedure is often employed to achieve the burst nucleation by rapid introduction of reagents into the reaction vessel. Alternatively, a heating strategy can be adopted, in which a reaction mixture is prepared at low temperature followed by heating to initiate the particle nucleation and growth. In this paper, we summarize briefly the recent progress in synthesizing monodispersed magnetic nanoparticles.

Magnetic Ferrite MFe_2O_4 ($M = Fe, Co, Mn, \text{etc}$) Nanoparticles

Magnetic ferrites, which adopt cubic spinel structures and have a general formula of MFe_2O_4 , are one of the most important classes of magnetic materials. In such ferrites, oxygen atoms exhibit face-centered cubic (fcc) close packing with M^{2+} and Fe^{3+} cations occupying either tetrahedral or octahedral interstices. Depending on the identity of the M^{2+} in the lattice, different ferrites can show distinctive magnetic properties.

Recently, a facile organic phase synthesis utilizing high temperature reaction of metal acetylacetones and 1,2-alkanediols was developed.⁴ For example, monodisperse 6 nm single-crystal Fe_3O_4 nanoparticles (**Figure 1a**) were synthesized by heating (300°C) a reaction mixture of $Fe(acac)_3$ (**Aldrich Prod. No. 413402**), 1,2-hexadecanediol (**Aldrich Prod. No. 213748**), oleic acid (OA) (**Aldrich Prod. No. O1008**), oleylamine (OAm) (**Aldrich Prod. No. O7805**) and benzyl ether (**Aldrich Prod. No. 108014**). The particle size could be tuned to 20 nm by seed-mediated growth using small particles as seeds. The recipe was readily extended to the synthesis of other ferrite (MFe_2O_4 , $M = Co, Mn, Ni, \text{etc}$)

particles by incorporating a stoichiometric amount of $M(acac)_2$ together with $Fe(acac)_3$ into the reaction mixture. The control of magnetic properties of different MFe_2O_4 is better illustrated in the 16 nm nanoparticles of Fe_3O_4 and $CoFe_2O_4$. The Fe_3O_4 particles are superparamagnetic at room temperature with a saturation magnetization (M_s) of 83 emu/g, close to the bulk value of magnetite. At lower temperature, the particles become ferromagnetic with coercivity (H_c) of 450 Oe at 10K. In comparison, the 16 nm $CoFe_2O_4$ particles (**Figure 1b**) exhibit a room temperature H_c of 400 Oe and a much larger H_c of 20 kOe at 10 K (**Figure 1c**).

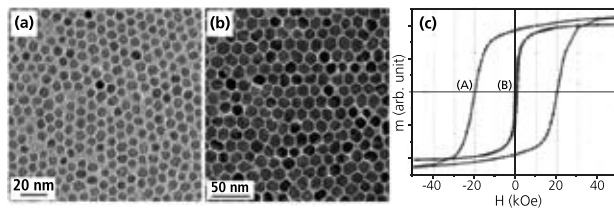


Figure 1. Transmission electron microscopy (TEM) images of (a) 6 nm Fe_3O_4 particles and (b) 16 nm $CoFe_2O_4$ particles; (c) Hysteresis loops of 16 nm $CoFe_2O_4$ particle assembly measured at A) 10 K and B) 300 K. Reproduced from Ref. 4 with permission from the American Chemical Society.

Fe_3O_4 nanoparticles can also be made by high temperature decomposition of iron(0) pentacarbonyl $Fe(CO)_5$ (**Aldrich Prod. No. 481718**) in presence of OA followed by oxidation using trimethylamine N-oxide ($CH_3)_3NO$ (**Aldrich Prod. No. 317594**) or air,⁵ or decomposition of metal-oletane complexes.⁶ Cube-like $MnFe_2O_4$ particles are synthesized by controlling the surfactant/precursor ratios.⁷ Ultra-small Fe_3O_4 nanoparticles are produced by thermal decomposition of $Fe(CO)_5$ in the presence of methyl catechol.⁸ Hollow Fe_3O_4 particles were fabricated by controlled oxidation of Fe/Fe_3O_4 particles utilizing the nanoscale Kirkendall effect.⁹

Metallic Fe and Co Nanoparticles

Metallic Fe (**Aldrich Prod. Nos. 637106, 544884**) and Co (**Aldrich Prod. No. 697745**) nanoparticles are important for various magnetic applications due to their high magnetization values (M_s : 218 emu/g for Fe and 162 emu/g for Co). However, fabrication of high moment Fe and Co nanoparticles has been very challenging due to their chemical instability. Recent syntheses prove that it is now possible to stabilize these reactive nanoparticles for high moment magnetic applications.



Scheme 1. Schematic outline of a facile synthesis of Fe nanoparticles via thermolysis of $Fe(CO)_5$ in 1-octadecene (ODE). Reprinted from Ref. 10 with permission from the American Chemical Society.

The most common approach for fabricating monodisperse Fe and Co nanoparticles is via thermal decomposition of the corresponding organometallic precursors, particularly the carbonyls. Recently, we reported a facile one-step synthesis (**Scheme 1**) of monodisperse Fe nanoparticles ($s < 7\%$) by thermolysis of $Fe(CO)_5$ in 1-octadecene (ODE) (**Aldrich Prod. No. O806**) with OAm.¹⁰ The primitive Fe particles were readily oxidized during post-synthesis treatment in air, giving



Chemical Synthesis of Monodisperse Magnetic Nanoparticles

8 nm/2.5 nm Fe/Fe₃O₄ nanoparticles (**Figure 2a**), with both the core and shell being amorphous. As-synthesized Fe/Fe₃O₄ particles are superparamagnetic at room temperature with M_s of ~67 emu/g. The value is normalized as 103 emu/g (Fe+Fe₃O₄) after surfactant removal and is close to the sum of the core- and the shell-contributions. Further oxidation of the particle dispersion in air led to rapid magnetic moment decline and severe particle agglomeration (Fig. 2c). However, once a dense shell of crystalline Fe₃O₄ was created over the Fe core via controlled oxidation using (CH₃)₃NO, Fe in Fe/Fe₃O₄ nanoparticles was more efficiently stabilized. The resulting core/shell nanoparticles of Fe/Fe₃O₄ (5nm/5nm) (**Figure 2b**) show an initial M_s of ~62 emu/g particles. Compared to the untreated particles, the moment of the oxidized particles drops much slower and is stabilized at 56 emu/g after 24 h exposure to air (**Figure 2c**). This crystalline Fe₃O₄ protection strategy has proved to be effective in stabilizing metallic Fe and giving stable core/shell nanoparticles of Fe/Fe₃O₄. Similarly, Co particles can be protected by a crystalline Fe₃O₄ shell as well.¹¹

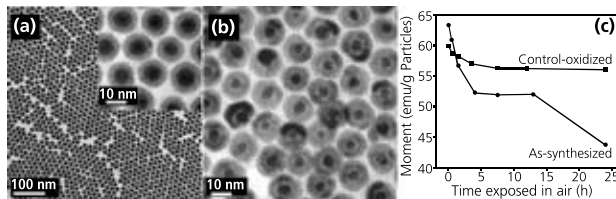


Figure 2. TEM images of (a) as-synthesized 8 nm/2.5 nm Fe/Fe₃O₄ nanoparticles, bar scale 100 nm (inset: higher resolution, bar scale 10 nm); (b) control-oxidized 5 nm/5 nm Fe/Fe₃O₄ particles, bar scale 10 nm. (c) The magnetic moment change of Fe/Fe₃O₄ core/shell particles versus time when exposed to air at room temperature. Reproduced from Ref. 10 with permission from the American Chemical Society.

Recent synthetic efforts have led to numerous other methods for making monodisperse Fe or Co nanoparticles. For example, 7 nm Fe nanocubes were made by thermolysis of [Fe(N(SiMe₃)₂)₂].¹² Hollow Fe nanoframes were formed via molten salt corrosion.¹³ Co particles with various crystal phases were synthesized by either cobalt carbonyl decomposition or cobalt salt reduction.¹⁴ Co nanorods were obtained by decomposition of [Co(η³-C₈H₁₃)(η⁴-C₈H₁₂)].¹⁵ Hollow Co particles were produced by simultaneous fast out-diffusion of CoO (**Aldrich Prod. No. 529443**) oxide species and surface reduction of the oxides by OAm.¹⁶

Magnetic Alloy Nanoparticles: FePt and FeCo

Magnetic iron-platinum (FePt) alloy nanoparticles made by solution-phase chemical synthesis have shown great potential for high performance permanent magnets and for high density data storage applications.¹ Their magnetic properties can be tuned not only by particle size, but also by their composition and structure. fcc-FePt nanoparticles have been fabricated by simultaneous decomposition of Fe(CO)₅ and reduction of Pt(acac)₂ (**Aldrich Prod. No. 523038**).¹⁷ The synthesis, annealing and alignment of shape-controlled FePt nanocubes and nanorods were also reported.^{17,18}

Very recently, dispersible fct-FePt particles were obtained via thermal annealing of MgO-coated fcc-FePt particles, followed by MgO removal.¹⁹ First, MgO (**Aldrich Prod. No. 529699**) was coated over the fcc-FePt surface via decomposition of Mg(acac)₂ (**Aldrich Prod. No. 129577**). The fcc-FePt/MgO nanoparticles were annealed to

800°C. The MgO shell was then removed via dilute acid washing and the fct-FePt particles were stabilized in hexane with a mixture of OA and 1-hexadecanethiol (**Aldrich Prod. No. 674516**). The coercivity of the fct-FePt particles reaches 2 T at 5K and 1 T at 300 K. The TEM images of the nanoparticles after each stage are shown in **Figures 3a thru 3c**.

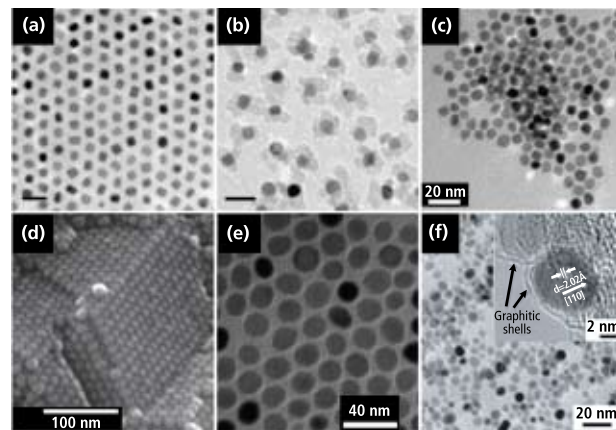


Figure 3. TEM images of: (a) as-prepared fcc-FePt particles (bar 20 nm), (b) MgO-coated and annealed FePt (bar 20 nm), (c) dispersible fct-FePt particles after shell removal and surface modification, reproduced from Ref. 19 with permission from Wiley-VCH, (d) 15 nm FeCo particles, reproduced from Ref. 20 with permission from the Nature Publishing Group, (e) 20 nm FeCo, reproduced from Ref. 21 with permission from the American Chemical Society, and (f) 7 nm FeCo particles, inset: HRTEM showing graphitic shell (bar 2nm), reproduced from Ref. 22 with permission from the Nature Publishing Group.

FeCo alloys have the highest magnetic moment under ambient conditions, reaching 245 emu/g. Uniform 15 nm FeCo alloy particles (**Figure 3d**) (M_s 160~180emu/g) were synthesized by co-decomposition of Fe(CO)₅ and Co(N(SiMe₃)₂).²⁰ 20 nm FeCo particles (**Figure 3e**) (M_s 207emu/g) were made by polyol co-reduction of Fe(III)- and Co(II)-acetylacetones (**Aldrich Prod. Nos. 517003 and 227129**) in OA/OAm under a reductive (Ar+7%H₂) atmosphere.²¹ Air-stable 7 nm FeCo particles (**Figure 3f**) with a graphitic shell were prepared via chemical vapor deposition, followed by surface modification using phospholipid-poly(ethylene glycol).²²

Rare-earth Metal Based Hard Nanomagnets of SmCo₅ and Nd₂Fe₁₄B

Rare-earth hard magnets, composed of rare-earth elements and 3d transition metals, are technically important permanent magnets. Two rare-earth systems, SmCo and NdFeB, have been at the center of hard magnetic research due to the need for nanocomposite magnets with enhanced coercivity and remnant magnetization for high performance permanent magnet applications. Traditional physical fabrication techniques, including melt spinning and ball milling, are often used to produce granular hard magnetic materials, but provide only limited control over the size of the final magnetic grains. Solution-phase chemical syntheses that have proven to be successful in preparing monodisperse magnetic nanoparticles were recently studied extensively for making nanostructured SmCo and NdFeB magnets.



Polyvinyl pyrrolidone (PVP) assisted co-reduction of Sm- and Co-nitrates in tetraethyleneglycol (TEG) (**Aldrich Prod. No. 110175**) were used to make the SmCo-magnets.²³ The resulting air-stable 10×100 nm blade-like rods (**Figure 4a**) were primarily hexagonal SmCo₅ with slight Sm₂Co₁₇ content. The intrinsic coercivity and magnetization of the particles were 6.1 kOe and 40 emu/g at room temperature, and 8.5 kOe and 44 emu/g at 10 K, respectively (**Figure 4b**). Nanocrystalline SmCo₅ (**Aldrich Prod. No. 692859**) hard magnets were also prepared by reacting core/shell structured Co/Sm₂O₃ particles (Co/Sm atomic ratio 4.3:1) with metallic Ca (**Aldrich Prod. No. 215147**) at 900 °C to reduce Sm₂O₃ and to promote interfacial diffusion between Sm and Co.²⁴ KCl (**Aldrich Prod. No. 409316**) was used as the dispersion medium to promote the reduction at relatively low temperatures and to prevent the sintering of SmCo₅ into large single-crystals. XRD confirmed the hexagonal SmCo₅ structure in the annealed product, while HRTEM revealed nanocrystalline grains (**Figure 4a**). The coercivity reached 24 kOe at 100 K and 8 kOe at room temperature with remnant moments of 40-50 emu/g (**Figure 4b**). The solution phase reaction and high temperature reduction process was extended to the synthesis of exchange-coupled SmCo₅/Fe_x nanocrystalline composites with a maximum coercivity of 11.6 kOe and remnant moment reaching 90 emu/g at room temperature (**Figures 4c and 4d**).²⁵

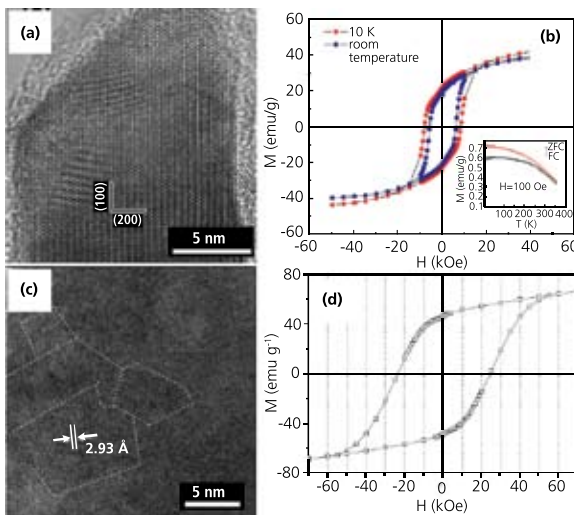


Figure 4. SmCo₅ magnets made from the PVP process: (a) HRTEM image (b) ambient and low temperature (10K) hysteresis loops, reproduced from Ref. 23 with permission from the American Institute of Physics. Nanocrystalline SmCo₅ via reductive annealing of Co/Sm₂O₃; (c) HRTEM image (d) 100 K magnetic measurement, reproduced from Ref. 24 with permission from Wiley-VCH.

Conclusion

A burst in the research efforts via chemical synthesis has led to the production of various monodisperse magnetic nanoparticles with controlled magnetic properties and chemical stability. In this short review, we have summarized recent exciting developments in some well-known magnetic nanoparticles of ferrites, metals, alloys and rare-earth magnets. These magnetic nanoparticles can be superparamagnetic ($H_c = 0$) or strongly ferromagnetic ($H_c > 1$ T) with magnetic moments ranging from those at the ferrite level of ~80 emu/g to the highest alloy value of over 200 emu/g. These magnetic nanoparticles have been studied extensively for various applications. For example, hard magnetic nanoparticles with large coercivity are promising for future ultra-high density information storage applications; soft magnetic nanoparticles with low coercivity and high magnetic moment are key components for electromagnetic devices. Composite nanoparticles containing exchange-coupled magnetically hard and soft phases are predicted to be the materials of choice for future permanent magnets with optimum energy product. Superparamagnetic nanoparticles have shown great potential for magnetic resonance imaging contrast enhancement and for magnetic fluid hyperthermia.

Acknowledgement

The magnetic research was supported by ONR/MURI N00014-05-1-0497 and DARPA/ARO W911NF-08-1-0249.

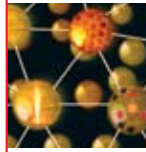
References:

- (1) Tarascon, M.A.; Kurihara, L.K.; Carpenter, E.E.; Calvin, S.; Harris, V.G. *Inter. Mater. Rev.*, **2004**, *49*, 125. (2) Cushing, B.L.; Kolesnichenko, V.L.; O'Connor, C.J. *Chem. Rev.*, **2004**, *104*, 3893. (3) Katz, E.; Willner, I. *Angew. Chem. Int. Ed.*, **2004**, *43*, 6042. (4) Sun, S.; Zeng, H.; Robinson, D.B.; Raoux, S.; Rice, P.M.; Wang, S.X.; Li, G. *J. Am. Chem. Soc.*, **2004**, *126*, 273. (5) Hyeon, T.; Lee, S.S.; Park, J.; Chung Y.; Na, H.B. *J. Am. Chem. Soc.*, **2001**, *123*, 12798. (6) Park, J.; An, K.; Hwang, Y.; Park, J.-G.; Noh, H.-J.; Kim, J.-Y.; Park, J.-H.; Hwang, N.-M.; Hyeon, T. *Nature Mater.*, **2004**, *3*, 891. (7) Zeng, H.; Rice, P.M.; Wang, S.X.; Sun, S. *J. Am. Chem. Soc.*, **2004**, *126*, 11458. (8) Xie, J.; Chen, K.; Lee, H.-Y.; Xu, C.; Hsu, A.R.; Peng, S.; Chen, X.; Sun, S. *J. Am. Chem. Soc.*, **2008**, *130*, 7542. (9) Peng, S.; Sun, S. *Angew. Chem. Int. Ed.*, **2007**, *46*, 4155. (10) Peng, S.; Wang, C.; Xie, J.; Sun, S. *J. Am. Chem. Soc.*, **2006**, *128*, 10676. (11) Peng, S.; Xie, J.; Sun, S. *J. Solid State Chem.*, **2008**, *181*, 1560. (12) Dumestre, F.; Chaudret, B.; Amiens, C.; Renaud, P.; Fejes, P. *Science*, **2004**, *303*, 821. (13) Kim, D.; Park, J.; An, K.; Yang, N.-K.; Park, J.-G.; Hyeon, T. *J. Am. Chem. Soc.*, **2007**, *129*, 5812. (14) Murray, C.B.; Sun, S.; Doyle, H.; Betley, T.A. *MRS Bull.*, **2001**, *985*. (15) Dumestre, F.; Chaudret, B.; Amiens, C.; Respaud, M.; Fejes, P.; Renaud, P.; Zurcher, P. *Angew. Chem. Int. Ed.*, **2003**, *42*, 5213. (16) Nam, K.M.; Shim, J.H.; Ki, H.; Choi, S.-I.; Lee, G.; Jang, J.K.; Jo, Y.; Jung, M.-H.; Song, H.; Park, J.T. *Angew. Chem. Int. Ed.*, **2008**, *47*, 9504. (17) Sun, S. *Adv. Mater.*, **2006**, *18*, 393. (18) Wang, C.; Hou, Y.; Kim, J.; Sun, S. *Angew. Chem. Int. Ed.*, **2007**, *46*, 6333. (19) Kim, J.; Rong, C.; Liu, J.P.; Sun, S. *Adv. Mater.*, DOI 10.1002/adma.200801620. (20) Desvaux, C.; Amiens, C.; Fejes, P.; Renaud, P.; Respaud, M.; Lecante, P.; Snoeck, E.; Chaudret, B. *Nature Mater.*, **2005**, *4*, 750. (21) Chaubey, G.S.; Barcena, C.; Poudyal, N.; Rong, C.; Gao, J.; Sun, S.; Liu, J. P. *J. Am. Chem. Soc.*, **2007**, *129*, 7214. (22) Seo, W.S.; Lee, J.H.; Sun, X.; Suzuki, Y.; Mann, D.; Liu, Z.; Terashima, M.; Yang, P.C.; McConnell, M.V.; Nishimura, D.G.; Dai, H. *Nature Mater.*, **2006**, *5*, 971. (23) Chinnasamy, C.N.; Huang, J.Y.; Lewis, L.H.; Latha, B.; Vittoria, C.; Harris, V.G. *Appl. Phys. Lett.*, **2008**, *93*, 032505. (24) Hou, Y.; Xu, Z.; Peng, S.; Rong, C.; Liu, J.P.; Sun, S. *Adv. Mater.*, **2007**, *19*, 3349. (25) Hou, Y.; Sun, S.; Rong, C.; Liu, J.P. *App. Phys. Lett.*, **2007**, *91*, 153117.

Magnetic Nanoparticles

For general metal precursors, see page 6. For noble metal precursors, see page 11.

Metallic Element Z: Symbol	Name	Composition	Magnetic Properties	Physical Form	Particle Size (nm)	Cat. No.
26: Fe	Iron oxide, magnetic nanoparticles solution	Fe ₃ O ₄	magnetization 30.6 emu/g (typical)	dispersion, 5 mg/mL in toluene	5 (average) 4.5-5.5 (TEM)	700320-5ML
26: Fe	Iron oxide, magnetic nanoparticles solution	Fe ₃ O ₄	magnetization 57.6 emu/g (typical)	dispersion, 5 mg/mL in toluene	9-11 (TEM) 10 (average)	700312-5ML
26: Fe	Iron oxide, magnetic nanoparticles solution	Fe ₃ O ₄	magnetization 80.1 emu/g (typical)	dispersion, 5 mg/mL in toluene	15 (average) 13.5-16.5 (TEM)	700304-5ML
27: Co	Cobalt, ≥99%	Carbon coated (magnetic) Carbon content < 8 wt. %	resistivity 6.24 μΩ·cm (20°C)	nanopowder	<50 (TEM)	697745-500MG
29: Cu	Copper iron oxide, 98.5% trace metals basis	CuFe ₂ O ₄	-	nanopowder	<100 (BET)	641723-10G 641723-50G
30: Zn	Zinc iron oxide, >99% trace metals basis	ZnFe ₂ O ₄	-	nanopowder	<100 (BET)	633844-10G 633844-50G
39: Y	Yttrium iron oxide, 99.9% trace metals basis	Y ₃ Fe ₅ O ₁₂	-	nanopowder	<100 (BET) <50 (XRD)	634417-10G



Chemical Synthesis of Monodisperse Magnetic Nanoparticles

Magnetic Metal Precursors

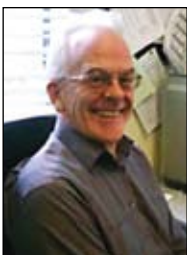
For general metal precursors, see page 6. For noble metal precursors, see page 11.

Metallic Element Z: Symbol	Name	Structure	Cat. No.
21: Sc	Tris[N,N-bis(trimethylsilyl)amide]scandium(III), 97%		547751-1G
24: Cr	Chromium(III) nitrate nonahydrate, 99.99+% trace metals basis	Cr(NO ₃) ₃ • 9H ₂ O	379972-5G 379972-25G
25: Mn	Manganese(0) carbonyl, 98%	Mn ₂ (CO) ₁₀	245267-1G 245267-10G
25: Mn	Manganese(II) nitrate hydrate, 99.99% trace metals basis	Mn(NO ₃) ₂ • xH ₂ O	203742-25G 203742-100G
25: Mn	Manganese(II) acetylacetone		245763-5G 245763-100G
26: Fe	Iron(0) pentacarbonyl, 99.999% trace metals basis	Fe(CO) ₅	481718-25ML 481718-100ML
26: Fe	Iron(III) nitrate nonahydrate, ≥99.999% trace metals basis	Fe(NO ₃) ₃ • 9H ₂ O	529303-25G
26: Fe	Iron(II) acetate, 99.995% trace metals basis		517933-5G 517933-25G
26: Fe	Iron(II) acetate, 95%		339199-10G 339199-50G
26: Fe	Iron(II) acetylacetone, 99.95% trace metals basis		413402-10G
26: Fe	Iron(III) ethoxide		697516-25ML
26: Fe	Iron(III) <i>tert</i> -butoxide dimer, 99.9% trace metals basis		698520-1G
27: Co	Cobalt(II) nitrate hexahydrate, 99.999% trace metals basis	Co(NO ₃) ₂ • 6H ₂ O	203106-10G 203106-50G
27: Co	Cobalt(II) acetate, 99.995% trace metals basis		399973-1G 399973-10G
27: Co	Cobalt(II) acetylacetone, 97%		227129-50G 227129-250G



Metallic Element Z: Symbol	Name	Structure	Cat. No.
28: Ni	Nickel(II) nitrate hexahydrate, 99.999% trace metals basis	$\text{Ni}(\text{NO}_3)_2 \cdot 6\text{H}_2\text{O}$	203874-20G 203874-100G 203874-500G
28: Ni	Nickel(II) acetate tetrahydrate, 99.998% trace metals basis	$\left[\text{H}_3\text{C}-\overset{\text{O}}{\underset{\text{O}^-}{\text{C}}}-\text{O}^- \right]_2 \text{Ni}^{2+} \cdot 4\text{H}_2\text{O}$	379883-10G 379883-50G
28: Ni	Nickel(II) acetylacetone, 95%	$\left[\text{H}_3\text{C}-\overset{\text{O}}{\underset{\text{O}^-}{\text{C}}}-\text{CH}_3 \right]_2 \text{Ni}^{2+}$	283657-5G 283657-25G 283657-50G
57: La	Lanthanum(III) nitrate hexahydrate, 99.999% trace metals basis	$\text{La}(\text{NO}_3)_3 \cdot 6\text{H}_2\text{O}$	203548-25G 203548-100G 203548-500G
57: La	Tris[N,N-bis(trimethylsilyl)amide]lanthanum(III), 98%	$\begin{matrix} \text{TMS}-\text{N}-\text{TMS} \\ \\ \text{TMS}-\text{N}-\text{La}-\text{N}-\text{TMS} \\ \\ \text{TMS}-\text{N}-\text{TMS} \end{matrix}$	547778-1G
58: Ce	Cerium(III) nitrate hexahydrate, 99.999% trace metals basis	$\text{Ce}(\text{NO}_3)_3 \cdot 6\text{H}_2\text{O}$	202991-25G 202991-125G
58: Ce	Cerium(III) acetylacetone hydrate	$\left[\text{H}_3\text{C}-\overset{\text{O}}{\underset{\text{O}^-}{\text{C}}}-\text{CH}_3 \right]_3 \text{Ce}^{3+} \cdot x\text{H}_2\text{O}$	381403-50G 381403-250G
58: Ce	Cerium(III) 2-ethylhexanoate	$\left[\text{H}_3\text{C}-\text{CH}_2-\text{CH}_2-\overset{\text{O}}{\underset{\text{O}^-}{\text{C}}}-\text{CH}_3 \right]_3 \text{Ce}^{3+}$	445576-5G 445576-25G
59: Pr	Praseodymium(III) nitrate hexahydrate, 99.99+% trace metals basis	$\text{Pr}(\text{NO}_3)_3 \cdot 6\text{H}_2\text{O}$	254053-5G
59: Pr	Praseodymium(III) acetylacetone hydrate, 99.9+% trace metals basis	$\left[\text{H}_3\text{C}-\overset{\text{O}}{\underset{\text{O}^-}{\text{C}}}-\text{CH}_3 \right]_3 \text{Pr}^{3+} \cdot x\text{H}_2\text{O}$	517674-5G 517674-25G
60: Nd	Neodymium(III) nitrate hydrate, 99.99% trace metals basis	$\text{Nd}(\text{NO}_3)_3 \cdot 6\text{H}_2\text{O}$	217204-25G
60: Nd	Neodymium(III) acetylacetone hydrate	$\left[\text{H}_3\text{C}-\overset{\text{O}}{\underset{\text{O}^-}{\text{C}}}-\text{CH}_3 \right]_3 \text{Nd}^{3+} \cdot x\text{H}_2\text{O}$	460427-10G 460427-50G
62: Sm	Samarium(III) nitrate hexahydrate, 99.999% trace metals basis	$\text{Sm}(\text{NO}_3)_3 \cdot 6\text{H}_2\text{O}$	518247-5G 518247-25G
62: Sm	Tris[N,N-bis(trimethylsilyl)amide]samarium(III), 98%	$\begin{matrix} \text{TMS}-\text{N}-\text{Sm}-\text{N}-\text{TMS} \\ \\ \text{TMS}-\text{N}-\text{TMS} \end{matrix}$	547980-1G
63: Eu	Europium(III) nitrate hydrate, 99.99% trace metals basis	$\text{Eu}(\text{NO}_3)_3 \cdot 5\text{H}_2\text{O}$	254061-1G 254061-10G
63: Eu	Europium(III) acetylacetone hydrate	$\left[\text{H}_3\text{C}-\overset{\text{O}}{\underset{\text{O}^-}{\text{C}}}-\text{CH}_3 \right]_3 \text{Eu}^{3+} \cdot x\text{H}_2\text{O}$	393215-1G 393215-5G
64: Gd	Gadolinium(III) nitrate hexahydrate, 99.99% trace metals basis	$\text{Gd}(\text{NO}_3)_3 \cdot 6\text{H}_2\text{O}$	451134-10G 451134-50G
64: Gd	Gadolinium(III) acetylacetone hydrate, 99.9% trace metals basis	$\left[\text{H}_3\text{C}-\overset{\text{O}}{\underset{\text{O}^-}{\text{C}}}-\text{CH}_3 \right]_3 \text{Gd}^{3+} \cdot 2\text{H}_2\text{O}$	331716-5G 331716-25G
65: Tb	Terbium(III) nitrate hexahydrate, 99.999% trace metals basis	$\text{Tb}(\text{NO}_3)_3 \cdot 6\text{H}_2\text{O}$	217212-2G 217212-10G
66: Dy	Dysprosium(III) nitrate hydrate, 99.9% trace metals basis	$\text{Dy}(\text{NO}_3)_3 \cdot x\text{H}_2\text{O}$	298158-25G 298158-100G
67: Ho	Holmium(III) nitrate pentahydrate, 99.99% trace metals basis	$\text{Ho}(\text{NO}_3)_3 \cdot 5\text{H}_2\text{O}$	229687-5G 229687-25G
68: Er	Erbium(III) nitrate pentahydrate, 99.9% trace metals basis	$\text{Er}(\text{NO}_3)_3 \cdot 5\text{H}_2\text{O}$	298166-25G 298166-100G
69: Tm	Thulium(III) nitrate pentahydrate, 99.9%	$\text{Tm}(\text{NO}_3)_3 \cdot 5\text{H}_2\text{O}$	325996-1G 325996-5G
70: Yb	Ytterbium(III) nitrate pentahydrate, 99.999%	$\text{Yb}(\text{NO}_3)_3 \cdot 5\text{H}_2\text{O}$	217220-5G 217220-25G
70: Yb	Tris[N,N-bis(trimethylsilyl)amide]ytterbium(III), 98%	$\begin{matrix} \text{TMS}-\text{N}-\text{TMS} \\ \\ \text{TMS}-\text{N}-\text{Yb}-\text{N}-\text{TMS} \\ \\ \text{TMS}-\text{N}-\text{TMS} \end{matrix}$	547875-1G

Starbons®: Cooking up Nanostructured Mesoporous Materials



Vitaly Budarin, James H. Clark*,
Rafael Luque, Robin White

Green Chemistry Centre, Department of
Chemistry, University of York, Heslington,
York YO10 5DD, UK

*Email: jhc1@york.ac.uk

Introduction

A mesoporous material is a material containing pores with diameters between 2 and 50 nm. The outstanding potential of mesoporous "carbonaceous" materials, in particular, has led to the search for a methodology that grants the desired control over surface chemistry and distribution of pore sizes; especially one that minimizes the formation of micropores, which are disadvantageous in applications that include chromatography¹ and catalysis.^{2,3} One approach that achieves this goal is the templating method. In a typical procedure,⁴ mesoporous silica is filled with a carbon precursor (e.g. sucrose), which is subsequently carbonized through a series of high temperature processes. The template is then removed using hydrofluoric acid or caustic soda. This method is multi-step, energy intensive, involves highly corrosive chemicals, and the resulting materials have a significant proportion of micropores. Nature can help with this; starch, for example, has a naturally, nano-channelled biopolymer structure which can be utilized as a template. Cooking starch in water opens its internal structure forming an accessible mesoporous network. This utilizes nature's ability to form nano-channelled biopolymer structures in the starch granules of plants.^{5,6} It was found that at low temperature, further treatment with acid and heating will then convert the expanded starch template into stable, nanostructured, mesoporous carbonaceous networks. This approach to the generation of nanostructures and new types of carbon-based materials with controllable physico-chemical properties helped us to produce the novel family of materials called Starbons.⁷⁻⁹ Because of their complex surface molecular structure, Starbons can be used in a variety of applications including chromatography, catalysis, environmental remediation, etc. and recently for making nanoparticles.

Starbon Synthesis

Our strategy is to synthesize mesoporous carbonaceous materials (hereinafter referred to as "Starbons") using mesoporous expanded starch⁷⁻⁹ as the precursor without the need for a templating agent. Starbon synthesis utilizes the natural ability of the amylose and amylopectin polymer chains within starch to assemble themselves into organized, largely mesoporous structures. The method comprises three key stages (**Figure 1**). Firstly, starch (typically from corn) is gelatinized by heating in water and subsequently cooled to 5 °C for one to two days to yield a porous gel block. The water in the block is then exchanged with ethanol, and oven dried to yield a predominantly mesoporous starch with a surface area of typically 180 m²g⁻¹.^{10,11} In the final stage, the mesoporous starch is doped with a catalytic amount of an organic acid (e.g. *p*-toluenesulfonic acid (**Aldrich Prod. No. 402885**)) and heated under vacuum.¹² A variety of mesoporous carbonaceous materials of controllable surface and bulk characteristics have been produced by heating to different temperatures ranging from 100-1400°C. These can be in a powder or a stable monolithic form as shown in Figure 1.



Starbons®: Cooking up Nanostructured Mesoporous Materials

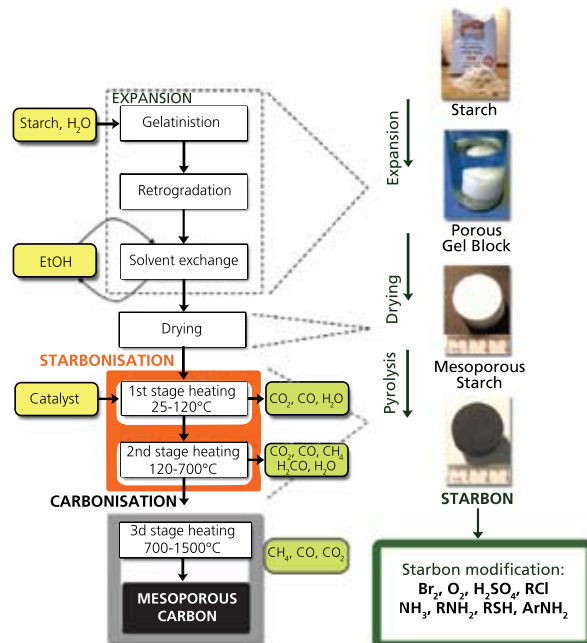


Figure 1. Method of Starbon preparation.



Starbon Properties

The porous structure of the Starbon comes from the expanded starch, which prevents the problem of micelle collapse that occurs in micelle templated polymer methods for the synthesis of mesoporous carbons,¹³ and removes the need for synthesis of mesoporous templates such as silica to define the structure. As illustrated in SEM pictures of Starbon and original mesoporous starch, the morphology of the sample particles during pyrolysis is largely preserved (**Figure 2**).

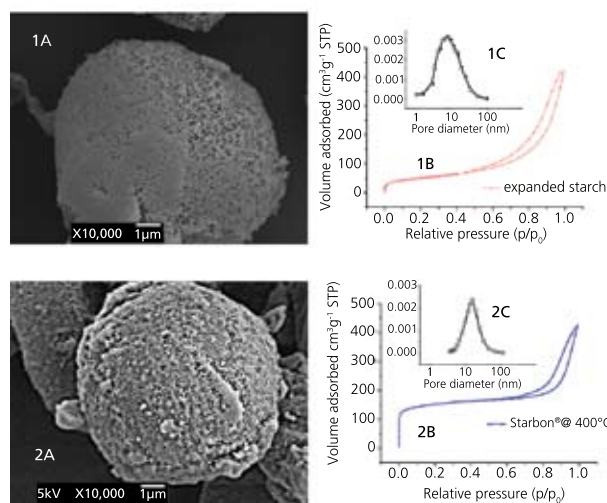


Figure 2. Textural properties of 1) mesoporous expanded starch a) SEM; b) isotherm of adsorption; c) BJH desorption isotherm and 2) Starbon prepared at 400°C a) SEM; b) isotherm of adsorption; c) BJH desorption isotherm.

The total pore volume and the average pore diameter in the mesoporous region remain essentially constant throughout the carbonization process. The average pore diameter in the mesoporous region is around 10 nm indicating a predominance of mesopores in the structure of Starbons®. Although there is a substantial increase in the contribution of the microporous region to the total surface area, the actual volume that this corresponds to is small in comparison to the total mesoporous volume (**Table 1**). These structural properties make Starbons particularly suitable for applications such as catalysis and chromatography.

The surface energy, E_{surface} , measured by the Dubinin-Astachov method, illustrates an overall increase as the preparation temperature rises. More starch-like properties are retained until about 150°C, above which there is gradual change toward carbon-like properties.^{9,14} X-ray photoelectron spectroscopy (XPS) further supports these observations indicating a nearly linear increase of carbon/oxygen ratio on the surface from 1.2 for expanded starch to 8.5 for Starbon prepared at 800°C (**Table 1**).

The carbonization trend is also reflected in the elemental analysis, although the ratios are slightly lower for the bulk (elemental analysis) than for the surface (XPS) of the materials. This suggests that the mechanism of the carbonization process initiates from the outer surface into the inner bulk of the material.

A greater carbon-like character imparts an increased thermal stability. Thermogravimetric analysis demonstrates that, when heated, the Starbons degrade to a lesser extent than starches (90% and 23% percent weight loss for starch and Starbon prepared at 450°C, respectively). Although the Starbons prepared at lower temperatures begin to decompose earlier than starch under the same conditions, the thermal stability and the onset decomposition temperatures increase with increasing carbon character eventually exceeding the values for starch.

The changes in the chemical composition that occur during the preparation of Starbons have also been investigated. Solid state ¹³C CP/MAS (cross-polarization/magic angle spinning) NMR spectra of the materials show that there are three main chemical changes in the transition from starch to Starbon. In the first step (150–200°C), a fraction of the -CH₂OH groups in the starch condense to form ether groups. In the second step (200–300°C) the remainder of the -CH₂OH groups in the starch condense to carbonyl groups conjugated with olefinic groups to form aliphatic and alkene/aromatic functions. In the third step (>300°C), the aliphatic groups are almost completely converted to aromatic p-systems. Diffuse reflectance FTIR spectroscopy confirms these findings; a progressive decrease in the concentration of -CH₂OH groups, and an increase in aliphatic and finally aromatic functionalities is evident.¹⁵ These changes are similar to those reported previously for ordinary starch, but here the corresponding steps occur at much lower temperatures.¹⁶

Table 1. Physical analysis of starch and Starbons.

Material	Surface Area m ² g ⁻¹		Pore Volume cm ³ g ⁻¹		C/O atomic ratio		E_{DA}^{d} kJ mol ⁻¹	Pore diameter (nm)
	BET	Mesoporous	Total	Mesoporous	EA ^c	XPS		
Ex-st ^a	184	160	0.62	0.61	1.20	1.10	7.4	7.6
Ex-st ₄₊ ^b	230	170	0.67	0.66	1.20	1.30	8.2	8.6
Starbon@100 °C	179	171	0.67	0.61	1.26	1.34	6.9	10.5
Starbon@150 °C	172	137	0.68	0.58	1.55	1.99	6.5	10.4
Starbon@220 °C	151	90	0.57	0.42	2.71	2.73	10.5	16
Starbon@300 °C	293	60	0.53	0.37	3.43	3.79	17.7	17.2
Starbon@350 °C	332	65	0.56	0.38	5.0	5.1	18.2	16.8
Starbon@450 °C	475	70	0.22	0.32	6.01	6.04	20.6	14.5
Starbon@600 °C	528	153	0.62	0.43	7.53	7.55	24.4	12.1
Starbon@700 °C	538	158	0.73	0.55	8.54	8.5	26.6	10.6
Starbon@800 °C	600	167	0.63	0.43	8.6	8.6	25.8	7.0

^a Expanded starch

^b Expanded starch doped

^c EA – elemental analysis

^d E_{DA} – Dubinin-Astachov energy



The properties of Starbons measured using TGA, ^{13}C MAS NMR, DRIFT and XPS spectroscopy are summarized in **Figure 3**. It can be seen that from a starch to graphite-like structure above 700°C, there is a progressive increase in the hydrophobicity of the functional groups present.

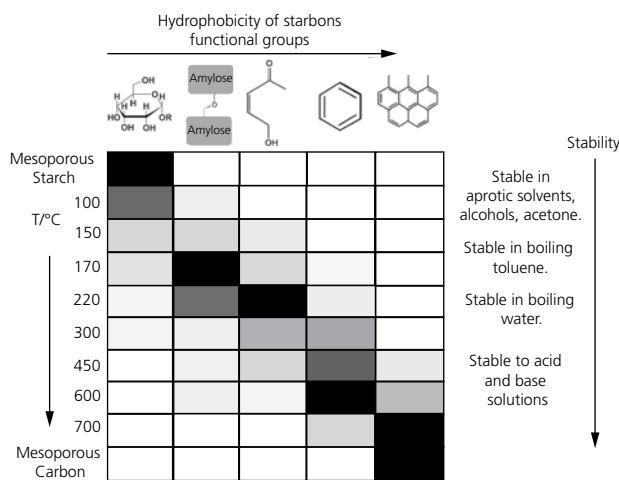


Figure 3. Influence of temperature of preparation on Starbon surface functionality.

It should be noted, that Starbons® prepared in the temperature range of 100–700°C also have a potential for chemical modification to alter their physical and chemical properties. The data obtained by ^{13}C MAS NMR and DRIFT spectroscopy indicate the presence of functional groups typical to both starch and carbons. This means that the materials may potentially be modified chemically using methodologies suitable for starch¹⁰ (e.g. silylation, alkylation, esterification, etherification, etc.) as well as those suitable for carbonaceous materials (e.g. bromination, amination, etc.),¹⁷ which offers future opportunities for novel hybrids.

Starbon Applications

Information about the mechanism of starch decomposition gives us an opportunity to predict the optimal temperature of Starbon preparation for a given application. The remaining starch functionality within Starbons at temperatures up to 250°C, enables the possible use of these materials in applications typical to starch such as the chromatographic separation of enantiomers.¹⁸ Preliminary studies have confirmed that they are effective as a stationary phase for liquid chromatography, allowing separation of a standard test mixture of substituted ferrocene compounds.

Low temperature prepared sulfonated aromatic carbonaceous materials have recently been shown to be effective solid acid catalysts. Since Starbons prepared between the temperatures of 300 and 600°C have aromatic functionality, sulfonation of these materials should also result in useful solid acid materials. Remarkably, we have found that reactions of carboxylic diacids in aqueous alcohol demonstrate the excellent activities and particular characteristics of Starbon acids.^{19,20} Esterification reactions of organic diacids in water were chosen because they can offer several interesting features. Firstly, (di)carboxylic acids are forecasted within the top biomass platforms for near future, large scale applicability. Secondly, esterifications are one of the most useful transformations for organic acids, especially for a dicarboxylic acid since the diester can be used as an intermediate in the manufacture of polymers. Thirdly, traditional esterification methods are unselective, and use soluble mineral acids that need to be separated at the end of the reaction, and lead to hazardous waste.

Starbon acids, based on Starbons prepared at different temperatures, show an optimum catalytic activity for each one of the diacids screened in the esterification, with sharply reduced activities below or above this maximum. Perhaps the most interesting feature of the Starbon acids catalysis is the substrate-dependent maximum temperature in catalytic activity (**Figure 4**); activities peaked at ca. 400°C for succinic acid (**Aldrich Prod. No. 398055**), 450°C for fumaric acid (**Aldrich Prod No. 240745**) and 550°C for itaconic acid (**Aldrich Prod. No. 129204**).

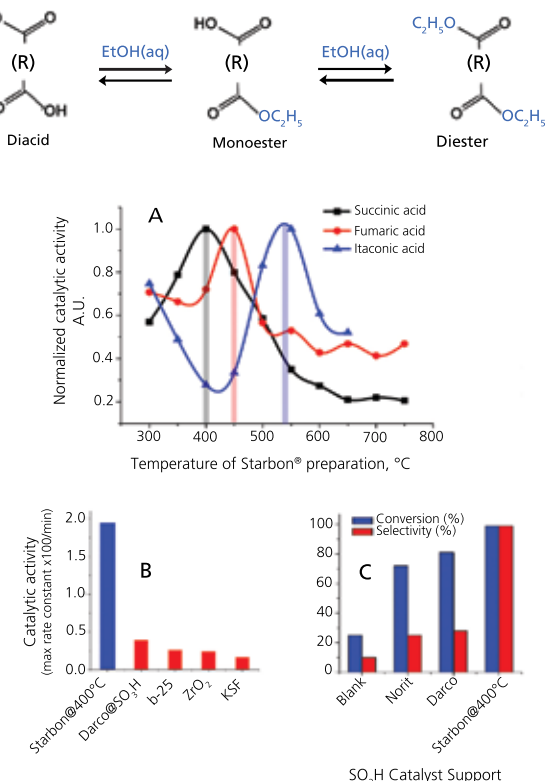


Figure 4. A) Normalized catalytic activity of Starbon acids in the esterification of succinic, fumaric and itaconic acids depending on the parent Starbon preparation temperature. Maximum catalytic activities were: Succinic acid (400°C, $k = 32 \times 10^{-5} \text{ s}^{-1}$); Fumaric acid (450°C, $k = 5.0 \times 10^{-5} \text{ s}^{-1}$); Itaconic acid (550°C, $k = 15.4 \times 10^{-5} \text{ s}^{-1}$). B) Starbon acid activity in reaction of succinic acid esterification as compared with typical inorganic solid catalysts. C) Starbon acid activity in reaction of succinic acid esterification as compared with SO_3H catalyst supports.

A further application for Starbons is as a solid carrier for precious metal catalysts. We have found that palladium metal supported on Starbons is an active catalyst for a model Heck reaction of iodobenzene (**Aldrich Prod. No. 17632**) with methyl acrylate (**Aldrich Prod. No. M27301**). Again, the importance of control over the surface chemistry of these materials is apparent; Starbons prepared at 220°C proved the most effective for this reaction.



Conclusion

We described a new approach to the generation of nanostructures that is simple, utilizes natural materials, and avoids difficult and energy-intensive synthetic steps that are common in existing templating methods, and results in a new type of carbon-based materials with readily controllable physico-chemical properties. The approach utilizes nature's ability to form nano-channelled biopolymer structures in starch granules of plants. The internal structure opens up by simply cooking starch in water and subsequently the biopolymer strands, through their natural self-organizing ability, assemble to form a starch block with an inherent mesoporous network. This mesoporous structure is then fixed by thermolysis to produce new materials that we named *Starbons*®. In addition to good chemical and mechanical stabilities, Starbons exhibit controllable surface energies, unusually high mesoporous volumes, and a complex surface molecular structure readily amenable to chemical functionalization. These properties make Starbons potentially useful in chromatography, catalysis, adsorption and many other applications.

Mesoporous Materials

Mesoporous Carbons

Name	Composition	Particle Size	Pore Structure	Spec. Surface Area (m ² /g)	Cat. No.
Carbon, mesoporous, Starbon® 300	C/O Ratio 3.2-3.6	-	mesoporosity 0.44-0.46 cm ³ /g microporosity ≥ 0.13 cm ³ /g, hydrophilic pore surface	>300 (BET) ≥130	702110-5G
Carbon, mesoporous, Starbon® 800	C/O Ratio 8.3-8.9	-	mesoporosity 0.4-0.7 cm ³ /g microporosity 0-0.2 cm ³ /g, hydrophobic pore surface	150-500 (BET)	702102-5G
Carbon, mesoporous	-	particle size distribution 45 ± 5 µm	average pore diameter 100 Å ± 10 Å pore volume 0.488 cm ³ /g	>200	699640-5G
Carbon	-	particle size <200 nm (DLS)	average pore diameter 64 Å total pore volume 0.342 cm ³ /g	>200	699632-5G
Carbon	-	particle size <200 nm (DLS)	average pore diameter 137 Å, graphitized	70	699624-5G

Starbon® is a registered trademark of the University of York.

Selected Mesoporous Materials

Name	Composition	Particle Size (µm)	Pore Structure Type	Pore Structure Dimension	Spec. Surface Area (m ² /g)	Cat. No.
Silica, mesostructured	SiO ₂	-	MCM-41 type (hexagonal)	pore size 2.3-2.7 nm pore volume 0.98 cm ³ /g	~1000 (BET)	643645-5G 643645-25G
Silica, mesostructured	SiO ₂	-	MSU-F (cellular foam)	pore volume 2.31 cm ³ /g	562	560979-10G
Silica, mesostructured	SiO ₂	3.05 (avg.)	HMS (wormhole)	pore size 3.9 nm (avg.) pore volume 1.76 cm ³ /g	910	541036-5G 541036-25G
Silica, mesostructured	SiO ₂	-	MSU-H (large pore 2D hexagonal)	pore size ~ 7.1 nm pore volume 0.91 cm ³ /g	~750 (BET)	643637-5G 643637-25G
Aluminosilicate, mesostructured	aluminum ~ 3%, (SiO ₂) _x (Al ₂ O ₃) _y	-	MCM-41 (hexagonal)	pore size 2.5-3 nm pore volume 1.0 cm ³ /g	940-1000 (BET)	643653-5G 643653-25G
Aluminosilicate, mesostructured	aluminum 3.0% (mol), (SiO ₂) _x (Al ₂ O ₃) _y	-	Al-MSU-F (cellular foam)	pore volume 2.03 cm ³ /g	605 (BET)	643629-5G 643629-25G
Aluminum oxide, mesoporous	-	5.65 (avg.)	MSU-X (wormhole) molecular sieve	average pore size 3.8 nm	-	517747-5G
Aluminum oxide, mesoporous	-	4.4 (avg.)	MSU-X (wormhole) molecular sieve	pore size 6.5 nm	-	517755-5G 517755-25G

Acknowledgements:

We thank the EPSRC for financial assistance and colleagues in the York Clean Technology Centre for their intellectual input. We thank Mr. P. Elliott, and Ms. M. Stark for their analytical support and advice.

References:

- (1) Poole, C. F. *The Essence of Chromatography*; Elsevier: New York (2003).
- (2) Sayari, A. *Chem.Mater.*, **1996**, 8, 1840.
- (3) Joo, S.H. et al., *Nature*, **2001**, 412, 169.
- (4) Ryoo, R.; Joo, S.H.; Jui, S. *J. Phys. Chem. B*, **1999**, 103, 7743.
- (5) Calvert, P. *Nature*, **1997**, 389, 338.
- (6) Daniels, D.R.; Donald, A.M. *Macromolecules*, **2004**, 37, 1312.
- (7) Starbon® is a registered trademark of the University of York.
- (8) Milkowski, K.; Clark, J.H.; Doi, S. *Green Chem.*, **2004**, 6, 189.
- (9) Budarin, V.; Clark, J.H.; Deswarth, F.E.I.; Hardy, J.J.E.; Hunt, A.J.; Kerton, F.M. *Chem.Commun.*, **2005**, 2903.
- (10) Doi, S.; Clark, J.H.; Macquarrie, D.J.; Milkowski, K. *Chem.Com.*, **2002**, 2632.
- (11) White, R.J.; Budarin, V.L.; Clark, J.H. *ChemSusChem*, **2008**, 1, 408.
- (12) Budarin, V.; Clark, J.H.; Hardy, J.J.E.; Luque, R.; Milkowski, K.; Tavener, S.J.; Wilson, A.J. *Anqw. Chem.*, **2006**, 45, 3782.
- (13) Lu, A.; Li, W.; Schmidt, W.; Schütt, F. *Micropor. Mesopor. Mater.*, **2005**, 80, 117.
- (14) Budarin, V.; Clark, J.H.; Tavener, S.J. *Chem. Commun.*, **2004**, 524.
- (15) Lua, A.; Yang, T. *J. Colloid Interf. Sci.*, **2004**, 274, 594.
- (16) Zhang, X.; Golding, J.; Burger, I. *Polymer*, **2002**, 43, 5791.
- (17) Budarin, V.; Clark, J.H.; Tavener, S.J.; Wilson, K. *C. Chem.Commun.*, **2004**, 23, 2736.
- (18) Hess, D. C. H.; Burger, G.; Musso, H. *Anqw. Chem.*, **1978**, 90, 645.
- (19) Budarin, V.L.; Clark, J.H.; Luque, R.; Macquarrie, D.J. *Chem.Commun.*, **2007**, 634.
- (20) Budarin, V.L.; Clark, J.H.; Luque, R.; Macquarrie, D.J.; Koutinas, A.; Webb, C. *Green Chemistry*, **2007**, 9, 992.

Manufacturing, Characterization and Use of Single Walled Carbon Nanotubes



Richard Jansen and Philip Wallis*
SouthWest NanoTechnologies, Inc.
2501 Technology Place
Norman, OK 73071
*Email: pwallis@swentnano.com

Introduction

Carbon nanotubes are materials that possess remarkable properties and offer extraordinary possibilities. This article gives a brief overview of the physico-chemical nature and characterization of single-walled nanotubes (SWNTs). We describe the current state of efforts to explore the SWNT promise and the status of their commercialization. Except for a brief introductory comparison, we do not cover their "cousins", the multi-walled carbon nanotubes (MWNTs).

Since their discovery in 1991 by Iijima¹, single walled carbon nanotubes have stimulated a great deal of activity in both the global research community and industry, and have inspired much investment in manufacturing methods, characterization and application development. The reasons for this are quite clear, given the remarkable properties these materials possess and the diversity of distinct species, each with its own unique variations in those properties.

SWNTs and MWNTs share some similarities, but also striking differences. MWNTs can be thought of as a series of single walled tubes nested within one another. There may be as few as 2, or as many as 100 plus concentric walls. Their diameters may, therefore, be as great as 50nm as opposed to 0.7 - 2.0 nm for a typical SWNT. Only the outer wall generally contributes significantly to the electrical and mechanical properties of MWNTs when used in composites, for example, affording the opportunity for much lower loading of SWNTs versus MWNTs. Of the two carbon nanotube types, single walled nanotubes are the more remarkable. They have outstanding strength, can be highly electrically conducting or semiconducting, may be as thermally conductive at room temperature as any other known material, have a very large surface area per unit mass, and have unique optical properties. This range of unique properties has opened the doors to advances in performance in a wide range of materials and devices.

Structure of Carbon Nanotubes

Single walled carbon nanotubes are an allotrope of sp² hybridized carbon, similar to fullerenes. The structure can be thought of as a cylindrical tube comprised of 6-membered carbon rings, as in graphite. The cylindrical tubes may have one or both ends capped with a hemisphere of the buckyball or fullerene structure.

An understanding of SWNT structure requires familiarity with the concept of nanotube chirality, since the chirality of a SWNT dictates many of its properties. A concept known as a Chirality Map, illustrated in **Figure 1**, has been developed as a tool for understanding chirality and its implications.

A SWNT can be envisioned as a sheet of graphite one atom thick rolled into a tube (see inset in Figure 1). The chirality describes both the orientation and diameter to which the sheet is rolled. Each SWNT on the chirality map is defined by two integers, (n,m). As indicated previously chirality defines many of the properties of the individual SWNT. For example, SWNT shown on the chirality map in blue are metallic in nature. These are tubes where n=m (armchair) or n - m = 3i, (where i is any integer.) Those depicted in yellow are semiconducting, displaying different band gaps depending on the length of the chiral vector.

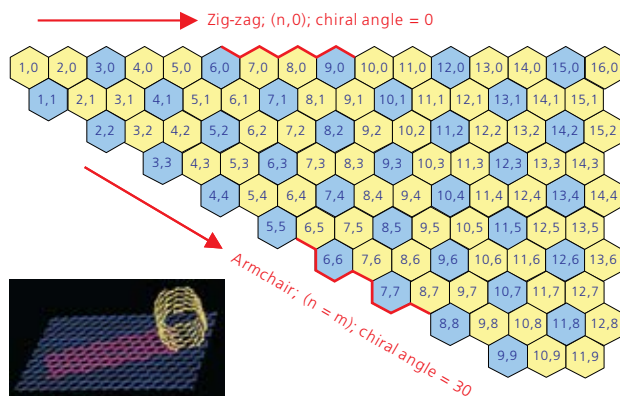


Figure 1. A graphic displaying a Chirality Map which shows the various types of SWNTs that can be formed. The properties are governed by the way in which they are rolled as shown in the insert. The SWNT will be metallic in the armchair configuration, or when m-n is a multiple of 3.

Unique Properties of Single Walled Carbon Nanotubes

Mechanical

Individual SWNTs are significantly stronger than steel. Calculated values for tensile strengths of SWNTs are ~ 100 times greater than steel at 1/16th the weight. The highest measured value is approximately half of the predicted theoretical strength,² possibly due to defects in the structure.

Electrical

Individual SWNTs, have current carrying capacities of 10⁹ amp/cm², higher than those of copper or gold,³ and semiconducting species exhibit higher electron mobility than silicon.

Optical

SWNTs have a distinct optical absorption and fluorescence response, with each chirality demonstrating its own characteristic absorption and fluorescence spectrum. In general, coating formed with SWNT are highly transparent in the visible and IR regions of the spectrum, making SWNT an ideal candidate to replace ITO as the transparent conductor of choice for applications such as displays, solar cells and electroluminescent lighting etc.

Thermal

Room temperature thermal conductivity of a single nanotube may be comparable to that of diamond or in-plane graphite, which are generally thought to display the highest measured thermal conductivity of any known material at moderate temperatures.





The Challenges of Single Walled Carbon Nanotubes (SWNTs)

Technical hurdles in the areas of purity, selectivity and dispersibility have so far limited the widespread application of SWNTs. Much recent progress has been made to address each of these obstacles.

Purity

The various manufacturing processes used in the production of SWNTs lead to products which are contaminated to varying degrees with residual catalyst and other forms of carbon. For many applications, secondary processes are necessary to remove these contaminants to provide product of sufficient purity. More recently, methods of synthesis that minimize the 'as manufactured' impurities have become commercially available.

Selectivity

As described earlier, the SWNTs are a mixture of tubes of different chiralities, some of which are electrically conducting and some are semiconducting. It is desirable, for many applications, to isolate the types of tubes from one another, such as metallic from semiconducting, and for some applications, tubes with well-defined individual chiralities (see previous section for an explanation of SWNT chirality). Laboratory scale methods designed to achieve a very high degree of selectivity have been reported,⁴ and efforts to develop scalable processes are underway. In particular, manufacturing processes such as the CoMoCAT® catalytic CVD process have been shown to provide a substantial degree of selectivity toward certain chiralities in as-synthesized SWNTs, making the yield of secondary purification processes substantially higher.

Dispersibility

SWNTs can be difficult to disperse, partly because of their well-known tendency to form ropes or bundles due to natural Van der Waals attraction between the tubes. However, they can be dispersed in aqueous solutions with the aid of suitable surfactants either as small bundles or as individual tubes. Exfoliation of bundles can be achieved by sonication of aqueous solutions of SWNTs in the presence of surface active molecules such as DNA, sodium deoxycholate (**Aldrich Prod. No. D6750**) and sodium cholate (**Aldrich Prod. No. 270911**). To quantify the degree of nanotube exfoliation obtained in a given dispersion, Tan and Resasco⁵ defined the concept of resonance ratio from the optical absorbance spectrum. The area of the resonant band divided by the area of the non-resonant background in this ratio allows easy comparison of results independent of the absolute absorption. Dispersants can then be ranked for their effectiveness using this parameter.

Additionally, dispersions of SWNTs in resins and thermoplastics is limited by a dramatic build up in viscosity caused by the entanglement of the SWNT bundles. Various proprietary methods exist to circumvent this problem, and new hybrid forms of SWNTs are being developed to address this issue.

SWNT Synthesis

Various methods have been used in the manufacture of SWNT. These include Laser Ablation, Carbon Arc and CVD processes, either involving a gaseous catalyst as in the HiPCo® process or using a supported catalyst as in the CoMoCAT process. The laser ablation process is used primarily for research materials. The Carbon Arc process produces long tubes with diameters in the range 1.4 to 2.0 nm, but carbon arc material has a very large amount of impurity and for most applications will require extensive purification. The CVD processes offer the best approach to the manufacturing of larger SWNT quantities, with perhaps the most scalable being the CoMoCAT process which uses a fluidized bed reactor (**Figure 2**) similar to those used in petroleum refining, albeit, on a much smaller scale.

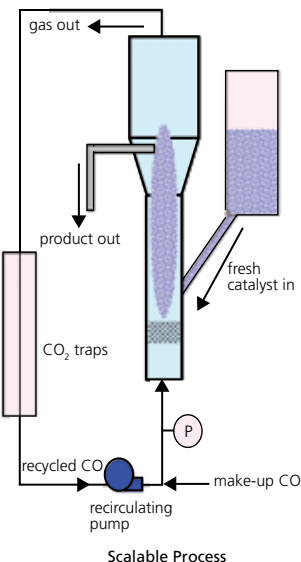


Figure 2. An illustration of a fluidized bed reactor which is able to scale up the generation of SWNTs using the CoMoCAT process.

In this CoMoCAT method, SWNT are grown by CO disproportionation (decomposition into C and CO₂) at 700–950°C in flow of pure CO at a total pressure that typically ranges from 1 to 10 atm. In a three-year research program of catalyst and reactor development, which included detailed characterization and testing of a large number of catalyst formulations and operating conditions, we developed a process that is able to grow significant amounts of SWNT in less than one hour, keeping a selectivity towards SWNT better than 90 percent. We discovered a synergistic effect between Co and Mo that is critical for the performance of the catalyst. The catalyst is effective when both metals are simultaneously present on a silica support with a low Co:Mo; separated, they are unselective. **Figure 3** shows the selective synthesis of a SWNT using the CoMoCAT method.

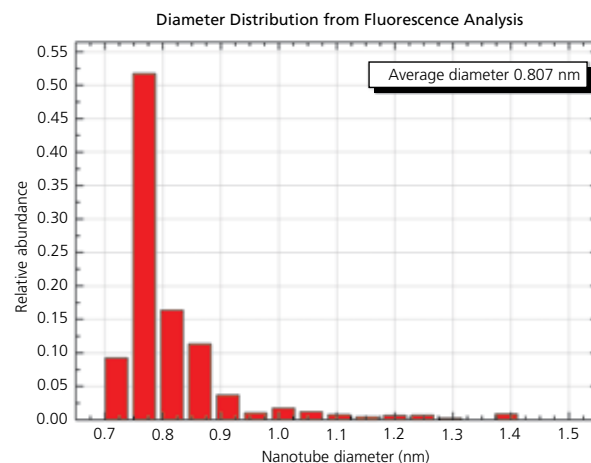


Figure 3. The Histogram for SG 65 material shows the very narrow distribution of SWNT diameters possible with the CoMoCAT process. 90% of the tubes have a diameter between 0.72 and 0.92 nm. 52% of the tubes are (6,5) chirality.

Two of the unique characteristics of the CoMoCAT process are that it is readily scalable and its intrinsic high selectivity is preserved as the reactor size is scaled up. These characteristics impart the SWNT product of the CoMoCAT process the dual benefit of low cost and high product quality. This supported catalyst approach also offers the unique ability to provide a substantial degree of chirality control during synthesis.

Characterization of SWNTs and Quality Assurance Parameters

As discussed above the properties of carbon nanotubes vary with the individual SWNT chirality. Since at this time all SWNTs are produced as a mixture of chiralities, the properties of the material will depend on the proportions of chiralities present. Many analytical techniques have been deployed to elucidate the structure of SWNT materials. These range from observational techniques such as SEM, TEM, AFM and STM to spectroscopic techniques such as UV-Vis-NIR, Photoluminescence, and Raman spectroscopy. In addition to these methods, X-ray diffraction has been used by Miyata et. al.⁶ to confirm the chirality assignments in the optical spectrum of SWNTs. Thermogravimetric analysis (TGA) has been used extensively to determine the onset of oxidation, maximum oxidation rate and the mass of catalyst retained in the product. In some cases it is possible to obtain a reasonable estimate of purity from the TGA curve.

TEM and SEM have been widely used to assess SWNT purity. However, these are unreliable for any quantitative estimation of purity. A typical TEM or SEM image uses ~ 1pg of material over an area of 1 to 4 μm^2 and it would therefore take the analysis of many micrographs imaged randomly throughout a macroscopic sample to obtain any meaningful results of the overall purity. Furthermore, there are no suitable algorithms for objectively determining the relative proportions of the different species seen in typical unpurified SWNT material. Thus, while TEM and SEM can give good information on the structure of the product, they must be used with caution and considered only as qualitative indicators of purity.

There are three relatively straightforward and commonly available techniques that can be used in combination to ensure that consistent high quality SWNTs are produced, namely Raman spectroscopy, Absorbance spectroscopy and Thermogravimetric analysis (TGA). Combined, these three methods give a good measure of purity and consistency of the SWNT. However, as SWNT applications are developed further, functional testing, such as electrical conductivity measurements, will be needed to link the purity data to SWNT performance.

Analysis by Raman Spectroscopy

Raman spectroscopy has been widely used for determining both the detailed combination of chiralities present in the SWNT material and for assessing purity. There are three areas of the Raman spectrum of primary interest for SWNTs. The Radial Breath Mode (RBM) from approximately 120 to 300 cm^{-1} is unique to SWNTs and can be used to determine tube diameter from the equation:

$$\nu = \frac{238}{d^{0.93}}$$

where, d is the SWNT diameter in nm and ν is the wavenumber in cm^{-1} .

It is important to note that to get a complete picture of the chiralities present, several lasers of different excitation frequency must be used. Using a continuously variable laser to excite the SWNT, Jorio, et.al. have mapped the chiral structure of SWeNT® SG 65.⁷

There are two additional bands seen in the Raman spectrum of SWNT: the D band at 1300 to 1350 cm^{-1} is indicative of disordered carbon, multiwall tubes and microcrystalline graphite, and the G band at 1500 to 1586 cm^{-1} is a result of the tangential stretching mode from graphitic-like materials. The ratio of the height of the G band to that of the D band has been widely used as a measure of the purity of SWNT. However, caution must be used when measuring this ratio as the G band is a resonant band and is therefore much stronger than the D band. It is probably best used by stating that a high G:D ratio is a necessary condition for high purity SWNT, but it is an insufficient assurance of purity since other methods must be used in conjunction with this parameter. For example, other forms of graphitic carbon may contribute to a strong G band.

The Raman G:D ratio, with the cautions listed above can be used as a first measure of purity. A typical Raman Spectrum for SWeNT SG 65 is shown in **Figure 4**. For quality assurance purposes, the RBM region can be used as a rough purity fingerprint.

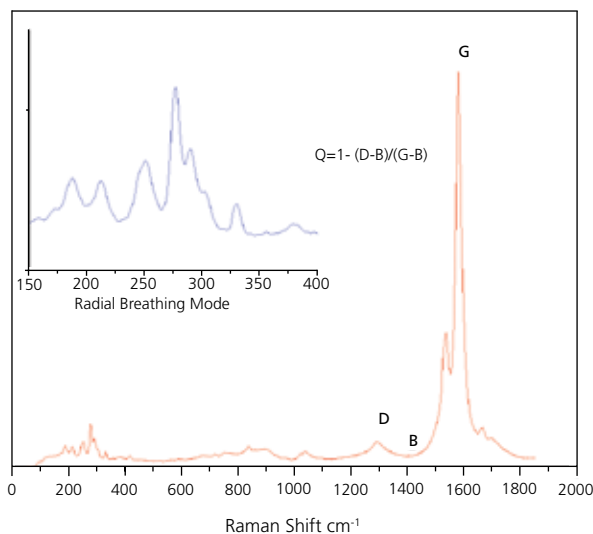
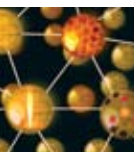


Figure 4. Typical Raman spectrum of SWeNT SG 65, obtained with 633 nm laser excitation.





Analysis by Optical Absorbance Spectroscopy

Optical absorption (OA) measurements in the UV-Vis.-NIR region show peaks which are characteristic of individual (n,m) species superimposed on the π -plasmon background. For example,⁸⁻⁹ the (6,5) species absorb at 566 and 976 nm and in response fluoresce at 983 nm. A (7,6) SWNT absorbs at 645 and 1024 nm and fluoresces in response at 1030 nm. These individual peaks have been used as a basis for estimating the purity of SWNT.¹⁰ Nair et. al.¹¹ have developed a method for computing the baseline for the spectrum, which then enables a calculation of peak heights and areas for the individual (n,m) species. For simplicity, we usually transform the measured OA spectrum to the energy domain, where the background becomes linear in the area of interest for SWNT characterization. **Figure 5** shows a typical OA spectrum for SWeNT® SG 65. The inset shows the spectrum in the more conventional form with the absorption plotted as a function of wavelength, while Figure 5b shows the same spectrum converted to the energy domain. Measurements of the height of the strongest peak, (P2B) and integration of the overall signal, S2B can be used to ensure that the product is consistent. We primarily use P2B as a control parameter for SWeNT® SG 65 and SG 76 nanotubes where one particular tube type is dominant. P2B is defined as the height of the highest peak in the spectrum between 350 and 1,350 nm divided by the background at that wavelength

$$P2B = \frac{\text{Height of (6,5) or (7,6) Signal Peak}}{\text{Height of Background Peak}}$$

It should be noted that the OA methodology as described here uses the OA spectrum measured after dispersing and centrifuging the SWNT sample. It is used as a measure of chirality control rather than overall purity. Measurement of the absorbance at a particular wavelength before and after centrifugation gives a measure of the dispersability of the SWNTs.

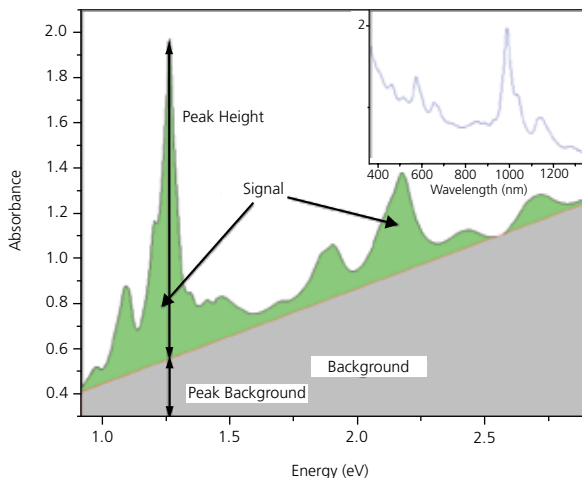


Figure 5. Optical Absorbance spectrum for SWeNT® SG 65. The highest peak corresponds to the (6,5) tubes.

Thermogravimetric Analysis

Thermogravimetric analysis (TGA) is used to assess the purity of the material. A typical TGA curve for SG 65 SWNT is shown in **Figure 6**. Studies have shown that the first peak in the derivative curve of the TGA trace represents the oxidation of SWNT, while the second peak is indicative of the presence of other forms of carbon. The quality parameters determined from the TGA analysis are T1% and residual mass at 625 °C.

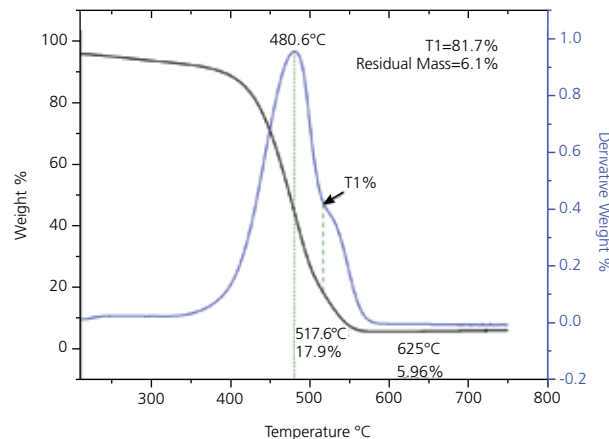


Figure 6. Thermogravimetric (TGA) Analysis for SWeNT® SG 65. The small peak in the derivative curve about 625 °C is due to changes in the residual catalyst as the material is heated.

T1%, as shown in **Figure 6**, is measured as a control parameter. It has been shown that this measurement typically underestimates the SWNT content by 3-5%. The position for T1 is taken at the minimum between the two peaks in the derivative curve. In the absence of a second distinct peak in the derivative curve, T1 is taken at the point of inflection. The weight loss % is recorded and the final value of T1% as a percentage of the carbon in the sample, corrected for the initial weight loss due to moisture in the sample is calculated from the following equation:

$$T1\% = \frac{\text{Initial weight} - \text{T1\% measured}}{\text{Initial weight} - \text{residual mass}}$$

The measurement of residual mass at 625 °C gives a measure of the non-carbon content of the material. The residual mass is expressed as a percentage normalized for the weight loss at 200 °C.

$$\text{Residual Mass} = \frac{\text{Weight Loss at } 625\text{ °C}}{\text{Initial Weight Loss}}$$

SWNT Applications

The numerous unique properties of SWNTs have led to their application in a wide range of technological problems.¹² Their extraordinary mechanical strength is exploited in enhanced carbon fiber¹³ and reinforced resins and elastomers; their highly conductive nature and large surface areas are utilized to prepare conductive polymer blends and films, improved lithium ion batteries, and super capacitors. Unique optical properties allow for their use as electrodes in displays, solarcells, and emerging solid state lighting technologies. The semiconducting nature of some SWNT species allow their adaptation to logic devices, non-volatile memory elements, sensors and security tags. It seems that new SWNT applications emerge regularly, limited only by the creativity of scientists and engineers working in the field.

Conclusion

Despite early excitement about SWNT materials and the extraordinary amount of research inspired by their discovery, to date, commercial exploitation of the technology has been disappointing. Perhaps there is insufficient understanding of the practical hurdles to their commercialization. However, momentum seems finally to be building, driven by substantial recent progress in these fundamental areas:

Metrology and Quality Control: The concept of "if you can measure it, you can improve it" applies here. The means are now available to adequately characterize SWNTs and to assure consistency of the materials needed for commercialization. Supporting this is the soon to be available offerings by NIST of Standard Reference Materials for calibration purposes.

Improved selectivity: Driven by applications that require more than a near-random distribution of tube chiralities, there has been a demonstration of the means to substantially narrow the 'as produced' chirality distributions of commercial scale production products. There is also promising work toward achieving further selectivity through secondary processing.

Dispersion: Recent years have seen the emergence of improved aids to disperse SWNTs for formulation in inks and composites.

Scale-up of manufacturing process: The last five years have seen development and a maturing of scalable SWNT manufacturing processes, which can provide commercial quantities of SWNT with high purity, controlled properties and consistent quality.

Trademarks: SWeNT® and CoMoCAT® are registered trademarks of Southwest Nanotechnologies, Inc. HiPCo® is a registered trademark of Carbon Nanotechnologies, Inc.

References:

- (1) Iijima, S. *Nature*, **1991**, 354, 56. (2) Meo, M.; Rossi, M. *Composite Science and Technology*, **2006**, 66, 1597. (3) Tans, S.J.; Devoret, H.; Thess, A.; Smalley, R.E.; Geerligs, L.J.; Dekker, C. *Nature*, **1997**, 386, 474. (4) Arnold, M.S.; Green, A.A.; Hulvat, J.F.; Stupp, S.I.; Hersham, M.C. *Nature Nanotechnology*, **2006**, 1, 60. (5) Tan, Y.; Resasco, D.E. *J. Phys. Chem. B*, **2005**, 109, 14454. (6) Miyata, Y.; Yanagi, K.; Maniya, Y.; Tanaka, T.; Kataura, H. *J. Phys. Chem. C*, **2008**, 112, 15997. (7) Jorio, A.; Santos, A.P.; Ribeiro, H.B.; Fantini, C.; Souza, M.; Viera, P.M.; Furtado, C.A.; Jiang, J.; Balzano, L.; Resasco, D.E.; Pimenta, M.A. *Phys. Rev. B*, **2005**, 72, 075207. (8) Bachilo, S.M.; Strano, M.S.; Kittrell, C.; Hauge, R.H.; Smalley, R.E.; Weisman, R.B. *Science*, **2002**, 298, 2361. (9) Lolli, G.; Zhang, L.; Balzano, L.; Sakulchaicharoen, N.; Tan, Y.; Resasco, D.E. *J. Phys. Chem. B*, **2006**, 110, 2108. (10) Itkis, M.E.; Perea, D.E.; Jung, R.; Niyoji, S.; Haddon, R.C. *J. Amer. Chem. Soc.*, **2005**, 127, 3439. (11) Nair, N.; Usrey, M.; Kim, W.-J.; Braatz, R.D.; Strano, M.S. *Anal. Chem.*, **2006**, 78, 7589. (12) Rensselaer Polytechnic Institute. Ajayan and Zhou. <http://www.rpi.edu/locker/38/001238/pdfs/applications%20of%20nanotubes.pdf>. (accessed Mar 03 2009). (13) Jorio, A.; Dresselhaus, G.; Dresselhaus, M.S. (Eds.). *Carbon Nanotubes, Topics in Applied Physics.*, Springer-Verlag, New York (2008).

Non-functionalized Carbon Nanotubes

For a complete list of nanotubes please visit sigma-aldrich.com/nanocarbon

Carbon Nanotubes, Single-Walled (SWNTs)

SWCNT Grade	Description	CNT Purity	Production Method	CNT Size	Cat. No.
SWeNT® CG-100	-	>75% carbon basis, carbon > 90%	Produced by CoMoCAT® catalytic CVD process	L 450-2300 nm (mode: 800nm; AFM), diameter 0.7 - 1.3 nm	704113-250MG 704113-1G
SWeNT® SG-76	(7,6) chirality	>80% carbon basis, carbon > 90%	Produced by CoMoCAT® catalytic CVD process.	L 300-2300 nm (mode: 800nm; AFM), diameter 0.7 - 1.1 nm	704121-250MG
SWeNT® SG-65	(6,5) chirality	>75% carbon basis, carbon > 90%	Produced by CoMoCAT® catalytic CVD process.	L 450-2000 nm (mode: 900nm; AFM), diameter 0.7 - 0.9 nm	704148-250MG
CarboLex AP-grade	-	50-70% carbon basis, carbon 50-70%	Produced by Arc method	diam. × L 1.2-1.5 nm × 2-5 µm (bundle dimensions)	519308-250MG 519308-1G
-	-	40-60 wt. % carbon basis, carbon ≥ 70%	Produced by Arc method	diam. × L 2-10 nm × 1-5 µm (bundle dimentions) 1.3-1.5 nm (individual SWNT diameter)	698695-1G 698695-5G

SWeNT® and CoMoCAT® are registered trademarks of Southwest Nanotechnologies.

Carbon Nanotubes, Multi-Walled (MWNTs)

CNT Type	CNT Purity	Production Method	CNT Size	Cat. No.
Carbon nanotube, double-walled	50-80% carbon basis, carbon > 90% (trace metal basis)	Produced by CVD method	O.D. × I.D. × L 5 nm × 1.3-2.0 nm × 50 µm	637351-250MG 637351-1G
Carbon nanotube, multi-walled	>90% carbon basis, carbon > 90%	Produced by CVD method	diam. × L 110-170 nm × 5-9 µm	659258-2G 659258-10G
Carbon nanotube, multi-walled	>90% carbon basis, carbon > 90% (trace metal basis)	Produced by Catalytic Chemical Vapor Deposition (CCVD)	O.D. × I.D. × L 10-15 nm × 2-6 nm × 0.1-10 µm	677248-5G 677248-25G
Carbon nanotube, multi-walled	>95% carbon basis, carbon content > 95% (trace metal basis)	Produced by CVD method.	O.D. × I.D. × L 7-15 nm × 3-6 nm × 0.5-200 µm , bundled	694185-1G 694185-5G 694185-25G
Carbon nanotube, multi-walled	>99% carbon basis, carbon > 99% (total metals impurities)	CVD followed by HCl demineralization	O.D. × L 6-13 nm × 2.5-20 µm 12 nm (average diameter, HRTEM) 10 µm (average length, TEM)	698849-1G





Carbon Nanotube Arrays

CNT Type	CNT Purity	Production Method	CNT Size	Surface Coverage	Substrate Dimensions	Cat. No.
Carbon nanotube array, multi-walled, vertically aligned on silicon wafer substrate	>99.9% carbon basis, Carbon content > 99.9% (structured (sp^2) carbon. <0.1% amorphous (sp^3) carbon.)	Produced by PECVD method (plasma-enhanced chemical vapor deposition)	diam. \times L 100 nm $\pm 10\%$ \times 30 μm $\pm 10\%$	surface coverage ~2 \times 10 ⁹ CNT/cm ² (~20/ μm^2)	(1cm X 1cm Si wafer substrate, {100}, 650-1000 μm thick, low n-doped (phosphorus), resistivity 1-30 ohm-cm.)	687804-1EA
Carbon nanotube array, multi-walled, vertically aligned on copper wafer substrate	>99.9% carbon basis, Carbon > 99.9% (structured (sp^2) carbon. <0.1% amorphous (sp^3) carbon.)	Produced by PECVD method (plasma-enhanced chemical vapous deposition)	diam. \times L 100 nm $\pm 10\%$ \times 30 μm $\pm 10\%$	surface coverage ~2 X 10 ⁹ CNT/cm ² (~20/ μm^2)	(1cm X 1cm X 0.05cm high conductivity low-oxygen copper substrate)	687812-1EA

Functionalized Carbon Nanotubes

CNT Type	CNT Purity	Extent Of Labeling	CNT Size	Solubility	Cat. No.
Carbon nanotube, single-walled, carboxylic acid functionalized	80-90% carbon basis	extent of labeling atom% carboxylic acid 3 - 6	diam. \times L 4-5 nm \times 0.5-1.5 μm (bundle dimensions)	DMF 1.0 mg/mL H ₂ O 0.1 mg/mL	652490-250MG 652490-1G
Carbon nanotube, single-walled, octadecylamine functionalized	80-90% carbon basis	extent of labeling 30 - 40 wt. % (ODA)	diam. \times L 2-10 nm \times 0.5-2 μm (bundle dimensions)	chloroform , soluble tetrahydrofuran >1 mg/mL methylene chloride , soluble carbon disulfide >1 mg/mL toluene, soluble benzene, soluble	652482-10MG 652482-100MG
Carbon nanotube, single-walled, poly(ethylene glycol) functionalized	80-90% carbon basis	extent of labeling 30 wt. % (PEG), M _w ~600 g/mol (PEG)	diam. \times L 4-5 nm \times 0.5-0.6 μm (bundle dimensions)	H ₂ O 5 mg/mL	652474-100MG
Carbon nanotube, single-walled, polyaminobenzene sulfonic acid functionalized	75-85% carbon basis	extent of labeling 65% (PABS, typical), average M _w 400-600 g/mol (PABS)	diam. \times L 1.1 nm \times 0.5-1.0 μm (bundle dimensions)	ethanol 0.05 mg/mL H ₂ O 5.0 mg/mL, As determined by near-IR absorbance spectroscopy. DMF 0.1 mg/mL	639230-100MG
Carbon nanotube, single-walled, amide functionalized	80-90% carbon basis	extent of labeling per 4 - 8 atom % (amide groups)	diam. \times L 4-6 nm \times 0.7-1.0 μm (bundle dimensions)	DMF 0.5-1.0 mg/mL, with sonication acetone 0.5-1.0 mg/mL, with sonication alcohols 0.5-1.0 mg/mL, with sonication	685380-100MG

Fullerenes

Name	Structure	Purity	Solubility	Cat. No.
Fullerene-C ₆₀		sublimed, 99.9%	organic solvents, soluble	572500-250MG 572500-1G
		99.5%	organic solvents, soluble	379646-100MG 379646-1G 379646-5G
		98%	organic solvents, soluble	483036-1G 483036-5G
[5,6]-Fullerene-C ₇₀		99%	benzene, soluble toluene, soluble	482994-10MG 482994-100MG 482994-500MG
Fullerene-C ₇₆	-	98%	-	482951-5MG
Fullerene-C ₈₄		98%	-	482986-5MG

What Matters in Materials Research? **Material Matters™**



Hot Topics • Expert Reviews

**A Technical Periodical from
Sigma-Aldrich Materials Science**

Recent thematic issues featured:

- Alternative Energy
- Biomaterials
- Nanoscale Surface Modification
- 3-D Nano and Micro Structures
- Advanced Metals and Alloys
- Organic Electronics
- Hydrogen Storage
- Advanced Applications of Engineering Nanomaterials

For a complimentary subscription to *Material Matters*
visit sigma-aldrich.com/mm2.

Sigma-Aldrich Materials Science—Your Chemistry Partner

sigma-aldrich.com

SIGMA-ALDRICH®

Manufacturing, Characterization and Use of Single Walled Carbon Nanotubes



Interactive Periodic Table

A roadmap to Aldrich Materials Science Products on the Web.

Click on your metal of interest to see major product groups.

- Metals
- Metal Oxides
- Salts
- Nanomaterials
- Organometallic Precursors

All 61 non-radioactive metals in the periodic table are available from Sigma-Aldrich.

Visit the Interactive Periodic Table at sigma-aldrich.com/periodic

sigma-aldrich.com

SIGMA-ALDRICH®

Sigma-Aldrich
3050 Spruce Street
St. Louis, MO 63103 USA
sigma-aldrich.com

Argentina
SIGMA-ALDRICH DE ARGENTINA S.A.
Free Tel: 0810 888 7446
Tel: (+54) 11 4556 1472
Fax: (+54) 11 4552 1698

Australia
SIGMA-ALDRICH PTY LTD.
Free Tel: 1800 800 097
Free Fax: 1800 800 096
Tel: (+61) 2 9841 0555
Fax: (+61) 2 9841 0500

Austria
SIGMA-ALDRICH HANDELS GmbH
Tel: (+43) 1 605 81 10
Fax: (+43) 1 605 81 20

Belgium
SIGMA-ALDRICH NV/S.A.
Free Tel: 0800 14747
Free Fax: 0800 14745
Tel: (+32) 3 899 13 01
Fax: (+32) 3 899 13 11

Brazil
SIGMA-ALDRICH BRASIL LTD.
Free Tel: 0800 701 7425
Tel: (+55) 11 3732 3100
Fax: (+55) 11 5522 9895

Canada
SIGMA-ALDRICH CANADA LTD.
Free Tel: 1800 565 1400
Free Fax: 1800 265 3858
Tel: (+1) 905 829 9500
Fax: (+1) 905 829 9292

Chile
SIGMA-ALDRICH
QUIMICA LIMITADA
Tel: (+56) 2 495 7395
Fax: (+56) 2 495 7396

China
SIGMA-ALDRICH (SHANGHAI)
TRADING CO. LTD.
Free Tel: 800 819 3336
Tel: (+86) 21 6141 5566
Fax: (+86) 21 6141 5567

Czech Republic
SIGMA-ALDRICH spol. s r. o.
Tel: (+420) 246 003 200
Fax: (+420) 246 003 291

Denmark
SIGMA-ALDRICH DENMARK A/S
Tel: (+45) 43 56 59 00
Fax: (+45) 43 56 59 05

Finland
SIGMA-ALDRICH FINLAND OY
Tel: (+358) 9 350 9250
Fax: (+358) 9 350 92555

France
SIGMA-ALDRICH CHIMIE S.à.r.l.
Free Tel: 0800 211 408
Free Fax: 0800 031 052
Tel: (+33) 474 82 28 00
Fax: (+33) 474 95 68 08

Germany
SIGMA-ALDRICH CHEMIE GmbH
Free Tel: 0800 51 55 000
Free Fax: 0800 64 90 000
Tel: (+49) 89 6513 0
Fax: (+49) 89 6513 1160

Greece
SIGMA-ALDRICH (O.M.) LTD.
Tel: (+30) 210 994 8010
Fax: (+30) 210 994 3831

Hungary
SIGMA-ALDRICH Kft
Ingyenes telefonszám: 06 80 355 355
Ingyenes fax szám: 06 80 344 344
Tel: (+36) 1 235 9055
Fax: (+36) 1 235 9050

India
SIGMA-ALDRICH CHEMICALS
PRIVATE LIMITED
Telephone

Bangalore: (+91) 80 6621 9400
New Delhi: (+91) 11 4358 8000
Mumbai: (+91) 22 2570 2364
Hyderabad: (+91) 40 4015 5488
Kolkata: (+91) 33 4013 8003
Fax

Bangalore: (+91) 80 6621 9650
New Delhi: (+91) 11 4358 8001
Mumbai: (+91) 22 2579 7589
Hyderabad: (+91) 40 4015 5466
Kolkata: (+91) 33 4013 8016

Ireland
SIGMA-ALDRICH IRELAND LTD.
Free Tel: 1800 200 888
Free Fax: 1800 600 222
Tel: (+353) 402 20370
Fax: (+353) 402 20375

Israel
SIGMA-ALDRICH ISRAEL LTD.
Free Tel: 1 800 70 2222
Tel: (+972) 8 948 4100
Fax: (+972) 8 948 4200

Italy
SIGMA-ALDRICH S.r.l.
Numero Verde: 800 827018
Tel: (+39) 02 3341 7310
Fax: (+39) 02 3801 0737

Japan
SIGMA-ALDRICH JAPAN K.K.
Tel: (+81) 3 5796 7300
Fax: (+81) 3 5796 7315

Korea
SIGMA-ALDRICH KOREA
Free Tel: (+82) 80 023 7111
Free Fax: (+82) 80 023 8111
Tel: (+82) 31 329 9000
Fax: (+82) 31 329 9090

Malaysia
SIGMA-ALDRICH (M) SDN. BHD
Tel: (+60) 3 5635 3321
Fax: (+60) 3 5635 4116

Mexico
SIGMA-ALDRICH QUÍMICA, S.A. de C.V.
Free Tel: 01 800 007 5300
Free Fax: 01 800 712 9920
Tel: (+52) 722 276 1600
Fax: (+52) 722 276 1601

The Netherlands
SIGMA-ALDRICH CHEMIE BV
Free Tel: 0800 022 9088
Free Fax: 0800 022 9089
Tel: (+31) 78 620 5411
Fax: (+31) 78 620 5421

New Zealand
SIGMA-ALDRICH NEW ZEALAND LTD.
Free Tel: 0800 936 666
Free Fax: 0800 937 777
Tel: (+61) 2 9841 0555
Fax: (+61) 2 9841 0500

Norway
SIGMA-ALDRICH NORWAY AS
Tel: (+47) 23 17 60 00
Fax: (+47) 23 17 60 10

Poland
SIGMA-ALDRICH Sp. z o.o.
Tel: (+48) 61 829 01 00
Fax: (+48) 61 829 01 20

Portugal
SIGMA-ALDRICH QUÍMICA, S.A.
Free Tel: 800 202 180
Free Fax: 800 202 178
Tel: (+351) 21 924 2555
Fax: (+351) 21 924 2610

Russia
SIGMA-ALDRICH RUS, LLC
Tel: (+7) 495 621 5579
Fax: (+7) 495 621 5923

Singapore
SIGMA-ALDRICH PTE. LTD.
Tel: (+65) 6779 1200
Fax: (+65) 6779 1822

Slovakia
SIGMA-ALDRICH spol. s r. o.
Tel: (+421) 255 571 562
Fax: (+421) 255 571 564

South Africa
SIGMA-ALDRICH (PTY) LTD.
Free Tel: 0800 1100 75
Free Fax: 0800 1100 79
Tel: (+27) 11 979 1188
Fax: (+27) 11 979 1119

Spain
SIGMA-ALDRICH QUÍMICA, S.A.
Free Tel: 900 101 376
Free Fax: 900 102 028
Tel: (+34) 91 661 99 77
Fax: (+34) 91 661 96 42

Sweden
SIGMA-ALDRICH SWEDEN AB
Tel: (+46) 8 742 4200
Fax: (+46) 8 742 4243

Switzerland
SIGMA-ALDRICH CHEMIE GmbH
Free Tel: 0800 80 00 80
Free Fax: 0800 80 00 81
Tel: (+41) 81 755 2828
Fax: (+41) 81 755 2815

United Kingdom
SIGMA-ALDRICH COMPANY LTD.
Free Tel: 0800 717 181
Free Fax: 0800 378 785
Tel: (+44) 1747 833 000
Fax: (+44) 1747 833 313

United States
SIGMA-ALDRICH
Toll-Free: 800 325 3010
Toll-Free Fax: 800 325 5052
Tel: (+1) 314 771 5765
Fax: (+1) 314 771 5757

Vietnam
SIGMA-ALDRICH PTE LTD. VN R.O.
Tel: (+84) 3516 2810
Fax: (+84) 6258 4238

Internet
sigma-aldrich.com



Mixed Sources
Product group from well-managed forests, controlled sources and recycled wood or fiber
www.fsc.org Cert no. SGS-COC-003338
© 1996 Forest Stewardship Council

World Headquarters
3050 Spruce St., St. Louis, MO 63103
(314) 771-5765
sigma-aldrich.com

Order/Customer Service (800) 325-3010 • Fax (800) 325-5052

Technical Service (800) 325-5832 • sigma-aldrich.com/techservice

Development/Custom Manufacturing Inquiries **SAFC®** (800) 244-1173

Accelerating Customers' Success through Innovation and Leadership in Life Science, High Technology and Service

©2009 Sigma-Aldrich Co. All rights reserved. SIGMA, SAFC, SAFC®, SIGMA-ALDRICH, ALDRICH, FLUKA, and SUPELCO, are trademarks belonging to Sigma-Aldrich Co. and its affiliate Sigma-Aldrich Biotechnology, L.P. Sigma brand products are sold through Sigma-Aldrich, Inc. Sigma-Aldrich, Inc. warrants that its products conform to the information contained in this and other Sigma-Aldrich publications. Purchaser must determine the suitability of the product(s) for their particular use. Additional terms and conditions may apply. Please see reverse side of the invoice or packing slip. Nafion is a registered trademark of E.I. du Pont de Nemours & Co., Inc. ESCAT is a trademark of Engelhard Corp. Eppendorf is a registered trademark of Eppendorf-Netheler-Hinz GmbH. Sepharose is a registered trademark of GE Healthcare. IGEPAL is a registered trademark of General Dyestuff Corp. Coomasie is a registered trademark of Imperial Chemical Industries Ltd. Plexcore is a registered trademark of Plextronics, Inc. NanoThinks and ProtoSilver are trademarks of Sigma-Aldrich Biotechnology LP and Sigma-Aldrich Co. Chromasolv, Pure-Pac and ReagentPlus are registered trademarks of Sigma-Aldrich Biotechnology LP and Sigma-Aldrich Co.